

#### **RESEARCH ARTICLE**

# A Cdc42 GEF, Gef1, through endocytosis organizes F-BAR Cdc15 along the actomyosin ring and promotes concentric furrowing

Udo N. Onwubiko<sup>1</sup>, Paul J. Mlynarczyk<sup>2</sup>, Bin Wei<sup>1</sup>, Julius Habiyaremye<sup>1</sup>, Amanda Clack<sup>1</sup>, Steven M. Abel<sup>2</sup> and Maitreyi E. Das<sup>1,\*</sup>

#### **ABSTRACT**

During cytokinesis, fission yeast coordinates actomyosin ring constriction with septum ingression, resulting in concentric furrow formation by a poorly defined mechanism. We report that Schizosaccharomyces pombe cells lacking the Cdc42 activator Gef1, combined with an activated allele of the formin, Cdc12, display non-concentric furrowing. Non-concentrically furrowing cells display uneven distribution of the scaffold Cdc15 along the ring. This suggests that, after ring assembly, uniform Cdc15 distribution along the ring enables proper furrow formation. We find that, after assembly, Cdc15 is recruited to the ring in an Arp2/3 complex-dependent manner and is decreased in the activated cdc12 mutant. Cdc15 at cortical endocytic patches shows increased levels and extended lifetimes in gef1 and activated cdc12 mutants. We hypothesize endocytosis helps recruit Cdc15 to assembled rings; uneven Cdc15 distribution at the ring occurs when endocytic patches contain increased Cdc15 levels and the patch-association rate is slow. Based on this, we developed a mathematical model that captures experimentally observed Cdc15 distributions along the ring. We propose that, at the ring, Gef1 and endocytic events promote uniform Cdc15 organization to enable proper septum ingression and concentric furrow formation.

KEY WORDS: Cdc42 GEF, Cdc15, Actomyosin ring, Arp2/3 complex, Endocytosis, Septum

#### **INTRODUCTION**

In animal and fungal cells, cytokinesis involves constriction of an actomyosin ring, which leads to furrow formation (Pollard and Wu, 2010). The fission yeast *Schizosaccharomyces pombe* assembles an actomyosin ring that constricts simultaneously with septum (cell wall) deposition, leading to membrane ingression and cleavage furrow formation (Lee et al., 2012; Pollard, 2010). Plenary work by several groups has explained in great detail the mechanism of actomyosin ring formation (Johnson et al., 2012; Lee et al., 2012; Pollard, 2014; Pollard and Wu, 2010) and constriction in fission yeast (Stachowiak et al., 2014; Thiyagarajan et al., 2015; Zhou et al., 2015). During furrow formation, the constricting actomyosin ring pulls in the membrane adjacent to it, forming a physical barrier

<sup>1</sup>Department of Biochemistry & Cellular and Molecular Biology, University of Tennessee, Knoxville, TN 37996, USA. <sup>2</sup>Department of Chemical and Biomolecular Engineering, University of Tennessee, Knoxville, TN 37996, USA.

\*Author for correspondence (mdas@utk.edu)

D B.W., 0000-0002-8088-3688; M.E.D., 0000-0001-9164-0158

turgor pressure to allow for membrane invagination and furrow formation (Proctor et al., 2012). Septum deposition behind the ingressing membrane, primarily mediated by the cell-wall synthesizing enzyme Bgs1, provides the force necessary to overcome turgor pressure (Cortés et al., 2002, 2007; Le Goff et al., 1999; Liu et al., 1999; Proctor et al., 2012). The type II myosins, Myo2 and Myp2, are the motors that pull on actin to mediate actomyosin ring constriction (Bezanilla et al., 2000; Kitayama et al., 1997; Mulvihill and Hyams, 2003; Sladewski et al., 2009). These myosins play a role in furrow formation even in the presence of an intact septum-building apparatus (Laplante et al., 2015). In addition, furrow formation requires membrane expansion at the site of division (Wang et al., 2016).

Whereas, in most animal cells, the actomyosin ring constricts

separating the two daughter cells. In cell-walled organisms like fission yeasts, the actomyosin ring must overcome high internal

immediately after assembly, in fission yeast the ring enters a maturation period (Bezanilla et al., 2000; Kamasaki et al., 2007; Laporte et al., 2010; Wu et al., 2003). During the maturation phase, the cell prepares for ring constriction, septum ingression and membrane expansion to enable furrow formation (Laporte et al., 2010; Wang et al., 2016). These processes are tightly coordinated, such that the furrow forms in a concentric manner, towards the central axis of the cell. Defects in the coordination of these processes could result in non-concentric furrow formation. It is not clear how these different events are spatio-temporally coordinated during cytokinesis. While the mechanistic events involved in maturation are not clearly understood, it is known that several cytokinetic proteins localize to the division site during this phase (Arasada and Pollard, 2014; Bezanilla et al., 2000; Muñoz et al., 2013; Ren et al., 2015; Wei et al., 2016). One of the proteins involved in maturation is the F-BAR-domain-containing protein Cdc15 that is critical for cytokinetic events after ring assembly (Arasada and Pollard, 2014; Cortés et al., 2015; Martin-Garcia et al., 2014; Ren et al., 2015). While Cdc15 is localized to the nodes during ring assembly (Carnahan and Gould, 2003; Fankhauser et al., 1995; Wu et al., 2003), once the ring forms, Cdc15 levels rapidly increase at the ring through an unknown mechanism (Wu and Pollard, 2005). Cdc15 has been shown to be required for septum formation, and cdc15 mutants lacking the scaffolding SH3 domain show defects in septum formation and recruitment of the Rho1 guanine-nucleotide exchange factor (GEF) Rgf3 (Marks et al., 1992; Ren et al., 2015; Roberts-Galbraith et al., 2009). Moreover, in cdc15 mutants, deposition of transitional endoplasmic reticulum at the division site is disrupted, and localization of Bgs1 is delayed (Arasada and Pollard, 2014; Cortés et al., 2015; Vjestica et al., 2008). In addition, coupled membrane trafficking events, such as exocytosis and endocytosis, occur near the division site after ring

assembly (Gachet and Hyams, 2005; Wang et al., 2016; Win et al., 2001). Soon after ring assembly, proteins involved in vesicle delivery and in endocytosis appear at the division site (Wang et al., 2016). Endocytic proteins such as the Arp2/3 complex, type I myosin Myo1, and fimbrin have been shown to localize to the division site and contribute to cytokinesis (McDonald et al., 2017; Pelham and Chang, 2002; Wang et al., 2016; Wu et al., 2001).

Previously, we reported that the small GTPase Cdc42 is activated at the site of cell division in a sequential manner during cytokinesis (Wei et al., 2016). In fission yeast, Cdc42 is activated by two GEFs, Gef1 and Scd1 (Chang et al., 1994; Coll et al., 2003). Gef1 at the membrane near the ring activates Cdc42 to promote timely onset of ring constriction and septum ingression (Coll et al., 2003; Hirota et al., 2003; Wei et al., 2016). This is followed by Scd1 localization to the ring, where it promotes efficient septum formation. Gef1 is required for timely recruitment of Bgs1 to the ring, while Scd1 recruits Bgs1 to the ingressing membrane during cleavage furrow formation (Wei et al., 2016). This suggests that Gef1 and Scd1 may function redundantly to localize Bgs1 to the division site. Indeed, while the individual deletion mutants of *gef1* and *scd1* are viable, the  $gefl\Delta scdl\Delta$  double mutant is inviable (Coll et al., 2003). Gefl localizes to the membrane adjacent to the constricting ring and is eventually lost once the ring disassembles (Wei et al., 2016). It is not clear how association of Gef1 with the actomyosin ring promotes timely constriction and septum ingression.

Here, we show that Gef1-mediated endocytic events promote concentric furrow formation. We find that a gef1 deletion mutation combined with an activated allele of the formin cdc12 results in nonconcentric membrane furrowing during cytokinesis. In these mutants, the rate of actomyosin ring constriction is not consistent along the circumference of the ring, with some regions constricting faster than others. While actomyosin ring assembly is normal in these mutants, Cdc15 is distributed unevenly along the ring. Regions of the ring with higher Cdc15 levels furrow faster than regions containing lower levels of Cdc15. Recruitment of Cdc15 at the ring after ring assembly is decreased in the activated formin mutants. We show that after assembly, disruption of Arp2/3complex-mediated endocytic actin patches result in lower levels of Cdc15 at the ring. We find that in gef1 deletion strains with an activated formin mutant, endocytic patches show slower dynamics and increased numbers of Cdc15. Our data show that Gef1 regulates endocytic patch dynamics in a Cdc42-dependent manner. We hypothesize that, after ring assembly, Cdc15 is recruited to the division site via endocytic actin patches. Slower Cdc15 patch dynamics and increased levels of Cdc15 in individual patches lead to its uneven distribution along the ring. Based on this hypothesis, we develop a mathematical model that recapitulates our experimental observations regarding Cdc15 distribution along the actomyosin ring. These findings suggest that Gef1-mediated Cdc42 activation and endocytic events regulate Cdc15 organization at the ring after assembly to promote concentric furrow formation.

#### **RESULTS**

## The actomyosin ring constricts non-concentrically in $gef1\Delta$ mutants expressing an activated formin mutant $cdc12\Delta503$

Gef1 is required for timely onset of ring constriction and septum ingression, and cells lacking gef1 display fewer actin cables during the ring stage of cytokinesis (Wei et al., 2016). The formin Cdc12 contributes to non-medial actin cable formation during cytokinesis (Huang et al., 2012). We tested whether an activated allele of the formin cdc12 would restore non-medial actin cables in  $gef1\Delta$  mutants and rescue the constriction defect. The formin mutant

 $cdc12\Delta503$  lacks a regulatory N-terminal domain and is an activated allele that displays an increase in total actin filaments (Coffman et al., 2013). We found that the mean number of non-medial actin cables was three in  $gef1^+cdc12^+$  cells, and two in  $gef1\Delta$ , four in  $cdc12\Delta503$  and five in  $gef1\Delta cdc12\Delta503$  mutants (Fig. 1A; Fig. S1A). In addition, compared to  $gef1^+cdc12^+$  cells,  $gef1\Delta$ ,  $cdc12\Delta503$  and  $gef1\Delta cdc12\Delta503$  mutants also displayed an increase in actin patch numbers away from the cell tips (Fig. 1A,B).

Contrary to our hypothesis, we found that the severity of ring constriction defects was increased in  $gefl\Delta$  mutants expressing the activated formin mutant cdc12Δ503 (Fig. S1B,D). We used the F-BAR-domain-containing protein Cdc15-GFP as an actomyosin ring marker and Sad1–mCherry as a spindle pole body marker to time different cytokinetic events.  $gef1\Delta cdc12\Delta 503$  cells display a remarkable phenotype in which the cleavage furrow failed to form concentric to the cell cortex. In these mutants, Cdc15-GFP-labeled rings tend to constrict to one side of the cell cortex instead of uniformly around the central axis. As a result, the furrow forms nonconcentrically from one side of the cell to the opposite side as observed by bright-field microscopy (Fig. 1D). In gef1<sup>+</sup>cdc12<sup>+</sup>cells, ring constriction and septum ingression are properly coordinated and display concentric furrowing. Non-concentric furrowing was observed in a small fraction of  $gefl\Delta$  and  $cdc12\Delta503$  mutants and in 61% of  $gef1\Delta cdc12\Delta 503$  mutants (Fig. 1E). These data suggest that Gef1 is required for robust cytokinesis and contributes to the process that ensures concentric furrow formation.

Furthermore, the timing of actomyosin ring formation in  $gef1\Delta$  and  $cdc12\Delta503$  cells was comparable to  $gef1^+cdc12^+$  and was only slightly delayed in  $gef1\Delta cdc12\Delta503$  mutants (Fig. S1C). As reported previously, when compared to  $gef1^+cdc12^+$  cells,  $gef1\Delta$  mutants display a delay in onset of ring constriction (Fig. S1B; Wei et al., 2016). Onset of ring constriction is further delayed in  $cdc12\Delta503$  and  $gef1\Delta cdc12\Delta503$  mutants. The rate of ring constriction was comparable in  $gef1^+cdc12^+$  and  $gef1\Delta$  cells, but slightly slower in  $cdc12\Delta503$  mutants. In contrast, the rate of constriction was over three-fold slower in  $gef1\Delta cdc12\Delta503$  mutants (Fig. S1D). These data demonstrate that ring constriction is impaired in  $gef1\Delta cdc12\Delta503$  mutants, likely resulting in non-concentric furrow formation.

## Cells with uneven distribution of the F-BAR protein Cdc15 at the ring display non-concentric ring constriction

Non-concentric furrow formation is a likely outcome of improper coordination of ring constriction and septum ingression. We followed constriction patterns of Cdc15–GFP-labeled actomyosin rings in  $gef1\Delta cdc12\Delta 503$  mutants over time to generate kymographs (Fig. 2A,a-d). We found that in gef1Δcdc12Δ503 mutants, the ring tends to constrict away from the central axis of the cell, as represented by the red dashed line, and display an irregular constriction rate along the ring (Fig. 2A,a–d). In gef1<sup>+</sup>cdc12<sup>+</sup> cells, however, the ring tends to constrict towards the central axis of the cell (Fig. 2A,e). In concentrically constricting rings, before the onset of ring constriction, protein distribution along the ring appears uniform (Fig. 2A,d,e). We measured the intensity of Cdc15–GFP at the two outer edges of the zprojected rings in the kymographs just before the onset of constriction. We calculated the fraction of Cdc15-GFP intensity at each edge in comparison to the sum of the intensities at the two edges of the ring. Rings in most gef1Δcdc12Δ503 mutant cells constrict non-concentrically (Fig. 1D) and the local concentration of Cdc15-GFP is higher in the parts of the ring that constrict faster (Fig. 2A–C). The fraction of gef1\(\Delta\cdc12\Delta503\) rings that displayed concentric furrow formation showed an equivalent distribution of Cdc15 intensity along the two edges of the z-projected ring (Fig. 2A,d,B).

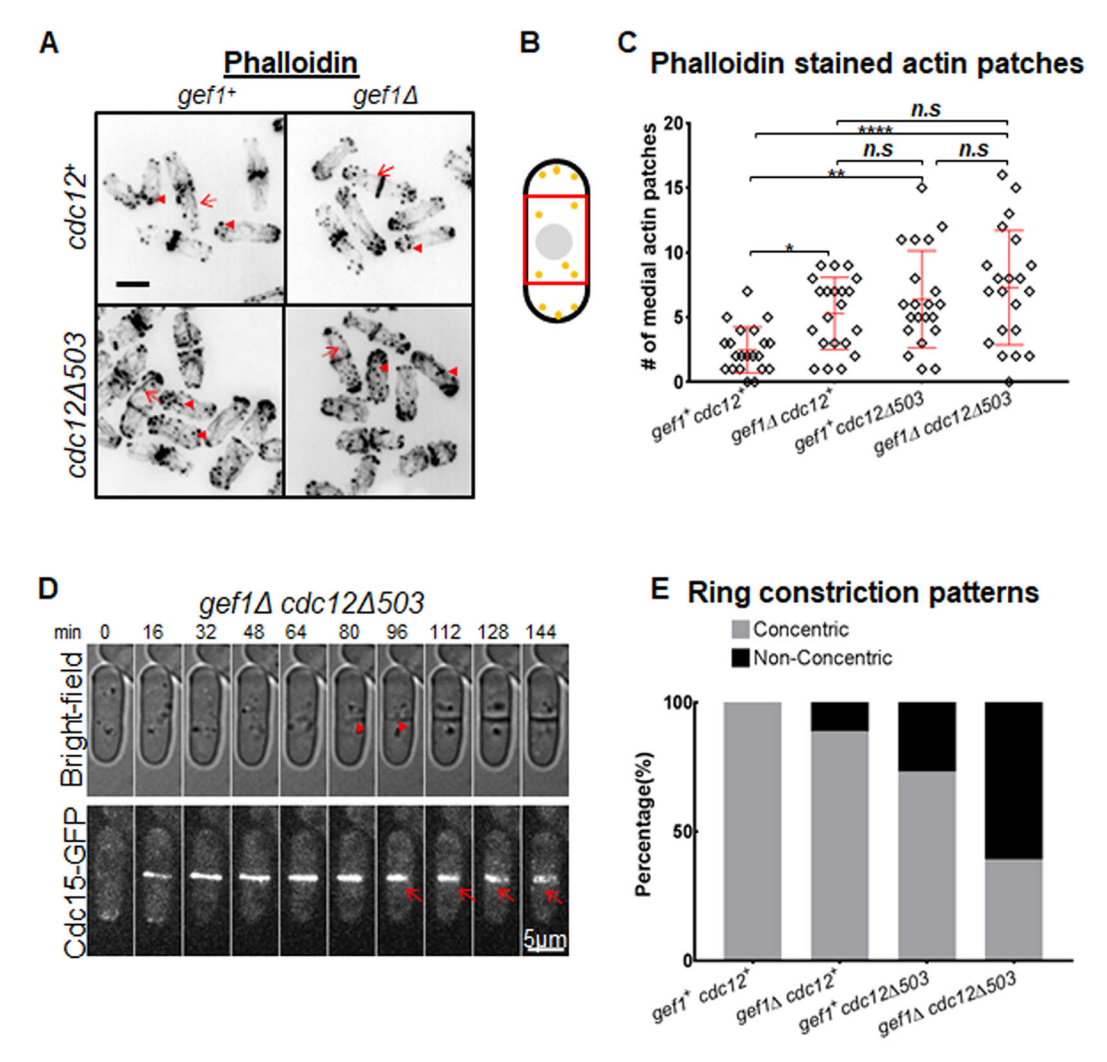


Fig. 1. The actomyosin ring constricts non-concentrically in  $gef1\Delta$  mutants expressing an activated formin mutant  $cdc12\Delta 503$ . (A) Phalloidin staining of actin cytoskeleton organization in strains as indicated. Red arrowheads point to actin patches, while red arrows indicate cables. (B) Schematic of a cell with disorganized actin patches (yellow circles). Non-medial patches depicted in the red box were counted. (C) Quantification of the number of non-medial actin patches in strains indicated [n=21 cells; \*P<0.05; \*\*P<0.01; \*\*\*\*P<0.001; \*\*\*\*P<0.0001; n.s., not statistically significant; one-way ANOVA (F(3,80)=8.218, P<0.0001) with Tukey's multiple comparisons post hoc test]. (D) Quantification of the percentage of gef1\* cdc12\* (n=17),  $gef1\Delta$  (n=27),  $cdc12\Delta 503$  (n=41) and  $gef1\Delta cdc12\Delta 503$  (n=28) cells with Cdc15–GFP-labeled rings showing non-concentric furrow formation. Error bars represent standard deviation. Scale bars: 5  $\mu$ m.

Our findings suggest that Cdc15 is irregularly distributed along the ring in  $gef1\Delta cdc12\Delta 503$  mutants, when compared to  $gef1^+cdc12^+$ ,  $gef1\Delta$  and  $cdc12\Delta 503$  cells. To test this, we divided the rings into four equal quadrants and measured the intensity of Cdc15–GFP in each quadrant, as previously described (Fig. 2E) (Wei et al., 2017). Next, we computed the coefficient of variation (CV) of the intensities of the quadrants of each ring. A higher coefficient of variation indicates more irregular distribution of proteins along the ring. We find that prior to the onset of constriction, the coefficient of variation in assembled rings was comparable in  $gef1^+cdc12^+$ ,  $gef1\Delta$  and  $cdc12\Delta 503$  cells (Fig. 2C,F). However, it was higher in  $gef1\Delta cdc12\Delta 503$  mutants (Fig. 2C,D,F), suggesting increased variation in Cdc15–GFP distribution in these rings. Thus, during non-concentric furrowing, faster-constricting sections of the ring contain higher levels of Cdc15–GFP.

Addition of a fluorescent tag to Cdc15 has been shown to affect its function (Cortés et al., 2015). It is therefore possible that non-concentric constriction is an artifact of Cdc15–GFP. Alternatively, irregular distribution of Cdc15–GFP along the ring in

 $gef1\Delta cdc12\Delta 503$  mutants could be due to defects in ring assembly or a structural anomaly in the actomyosin ring. To rule out these possibilities, we analyzed rings in  $gef1^+cdc12^+$ ,  $gef1\Delta$ ,  $cdc12\Delta503$ and gef1Δcdc12Δ503 cells expressing LifeAct-3×mCherry or the type II myosin light chain Rlc1-TdTomato. Under our imaging conditions, we did not find any structural anomaly in the actomyosin ring in these cells (Fig. 3A,B). We next analyzed the distribution of actin and Rlc1 along the ring in these cells, as performed above for Cdc15–GFP. We measured the intensity of LifeAct–3×mCherry and Rlc1-tdTomato in the four quadrants of the actomyosin ring and computed the CV, which is comparable in  $gef1^+cdc12^+$ ,  $gef1\Delta$ ,  $cdc12\Delta503$  and  $gef1\Delta cdc12\Delta503$  cells (Fig. 3C,D). We then analyzed constriction patterns in  $gef1^+cdc12^+$ ,  $gef1\Delta$ ,  $cdc12\Delta503$ and  $gef1\Delta cdc12\Delta 503$  cells expressing Rlc1-tdTomato. We find that even though gef1\Deltacdc12\Delta503 mutants display uniform Rlc1-TdTomato distribution along the ring, ~65% of the cells show nonconcentric constriction, similar to what was observed in cells expressing Cdc15-GFP (Fig. 1D; Fig. S1E). This suggests that in  $gef1\Delta cdc12\Delta 503$  mutants, merely fluorescently tagging Cdc15 does

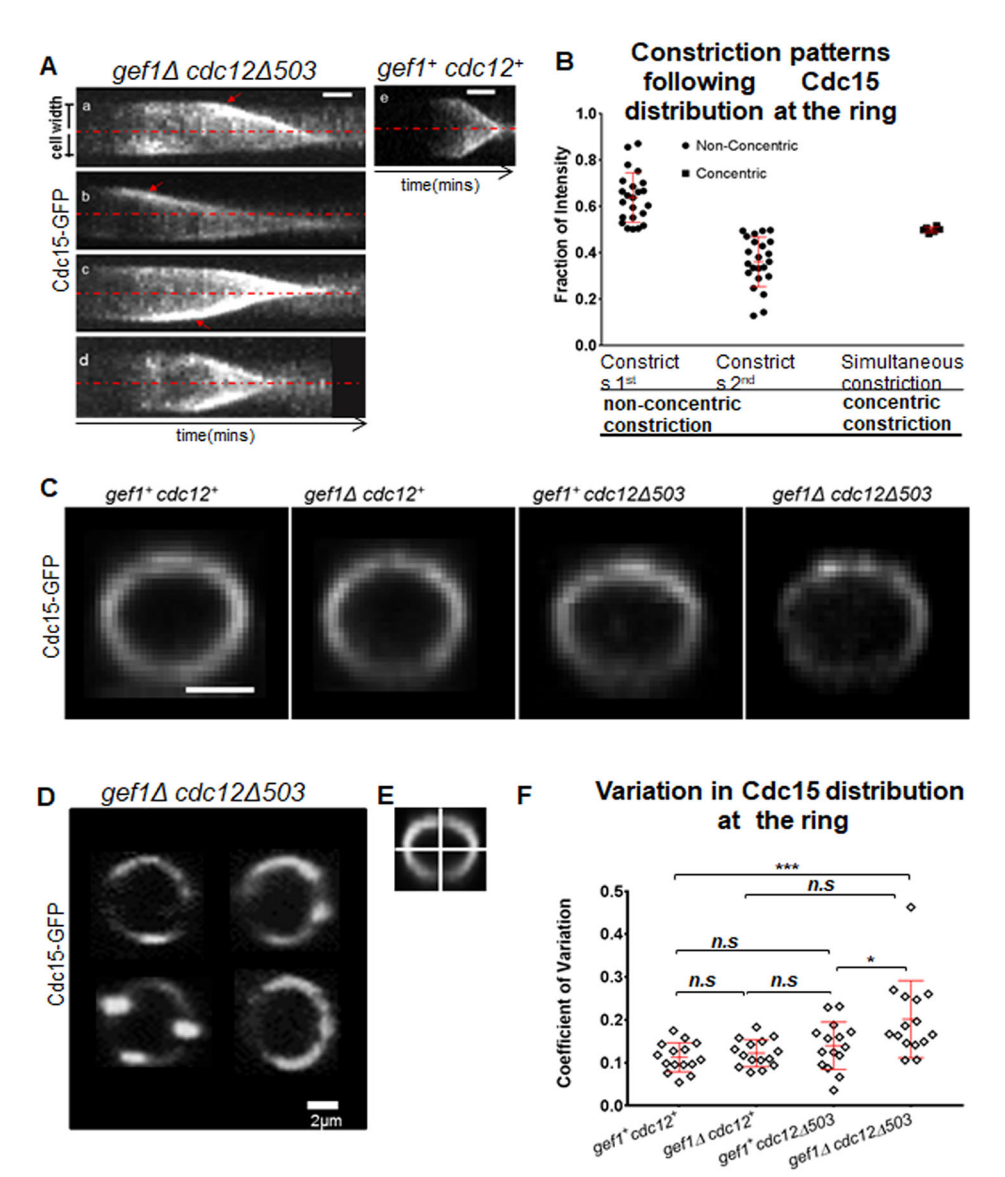


Fig. 2. Cells displaying non-concentric furrow formation exhibit uneven Cdc15 distribution along the ring. (A) Kymographs from time-lapse movies showing constriction of Cdc15–GFP-labeled rings in *gef1∆cdc12∆503* and gef1+cdc12+ cells. Red dashed lines indicate the central axis of the cells. Red arrows show regions of the ring constricting faster. (B) Quantification of the fraction of Cdc15-GFP intensity at different regions of the ring immediately prior to the onset of constriction. In kymographs of the cells constricting nonconcentrically, the side of the ring constricting first was compared to the side that constricted second. Rings constricting concentrically displayed simultaneous constriction of both sides of the kymograph. n=25 cells. (C) 3D-reconstructed Cdc15-GFP-labeled actomyosin ring of the indicated strains. (D) Examples of Cdc15–GFP distribution along the ring in gef1∆cdc12∆503 cells. (E) Illustration of actomyosin ring quadrants used for analyzing the CV of Cdc15-GFP distribution. (F) Quantification of the CV of Cdc15-GFP distribution in the indicated strains [n=15 cells; \*P=0.025, \*\*P=0.0023, \*\*\*P=0.0005; n.s., not statistically significant; one-way ANOVA (F(3,56)=7.163, P=0.0004), with Tukey's multiple comparisons post hoc test]. Error bars represent standard deviation. Scale bars: 2 µm.

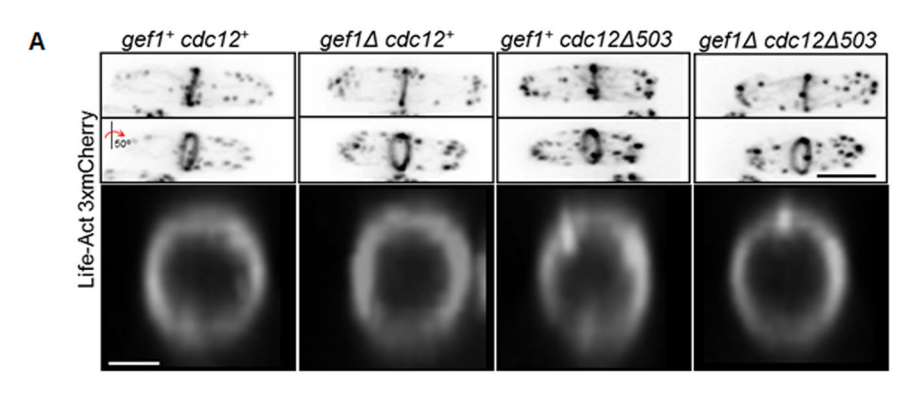
not lead to constriction defects and that non-concentric constriction occurs even though the rings properly organize the type II myosin light chain. Unfortunately, fluorescently tagging Cdc15 and Rlc1 or LifeAct simultaneously in  $gef1\Delta cdc12\Delta 503$  mutants did not result in viable cells. This prohibited simultaneous analysis of Cdc15 and actin/myosin distribution along the ring in  $gef1\Delta cdc12\Delta 503$  mutants.

Cdc15 appears at precursor nodes and interacts with Cdc12 (Carnahan and Gould, 2003; Willet et al., 2015). The  $cdc12\Delta503$  allele is a truncated mutant (Coffman et al., 2013) that lacks the Cdc15-interacting site (Willet et al., 2015). Irregular distribution of Cdc15 could be explained by the lack of this interaction. To test this, we analyzed Cdc15–GFP distribution along the ring in cdc12P31A mutants in a  $gef1\Delta$  background. The cdc12P31A mutant allele lacks the Cdc15-interacting site and fails to bind this protein  $in\ vitro$  (Willet et al., 2015). We found that the coefficient of variation of Cdc15–GFP in  $gef1\Delta cdc12P31A$  rings was comparable to that of the rings in  $gef1^+cdc12^+$ ,  $gef1\Delta$  and cdc12P31A cells (Fig. S2A). This indicated that the irregularity in Cdc15 distribution at the ring in  $gef1\Delta cdc12\Delta503$  mutants is not due to the lack of Cdc12–Cdc15 protein interaction. To understand how Gef1 regulates Cdc15 organization in the ring, we looked at known downstream targets of

Gef1. Gef1 activates Cdc42, which in turn activates the PAK kinase Pak1 (also known as Orb2 and Shk1) (Marcus et al., 1995; Parrini et al., 2002; Tu and Wigler, 1999). Cdc15 is a highly phosphorylated protein and, when de-phosphorylated, it forms oligomers via the BAR domain and establishes proper interaction with the membrane (Roberts-Galbraith et al., 2010). To test whether irregularities in Cdc15 distribution along the ring are due to absence of Pak1-dependent phosphorylation, we analyzed Cdc15 distribution along the ring in the pak1 mutant allele orb2-34 and  $orb2-34cdc12\Delta503$  mutants. The CV for Cdc15 distribution along the ring was not altered in orb2-34 or  $orb2-34cdc12\Delta503$  mutants in comparison to  $orb2^+cdc12^+$  cells (Fig. S2B). This indicates that irregularities in Cdc15 distribution along the ring in  $gef1\Delta cdc12\Delta503$  mutants are not due to the lack of Pak1 kinase activity.

## Activated cdc12 mutants display reduced Cdc15 levels in the ring

While Cdc15 localizes to the precursor nodes, after assembly of the ring, the numbers of Cdc15 in the ring increase until the onset of constriction (Wu and Pollard, 2005). Previous reports have shown that Cdc15 is a highly abundant protein at the ring and exchanges



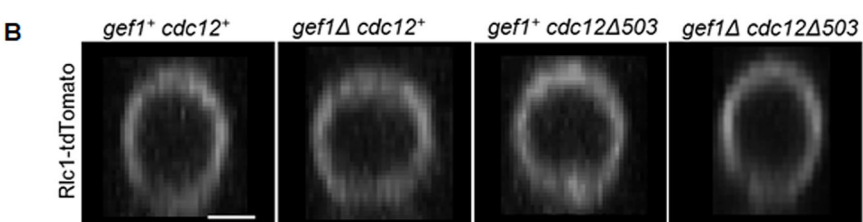
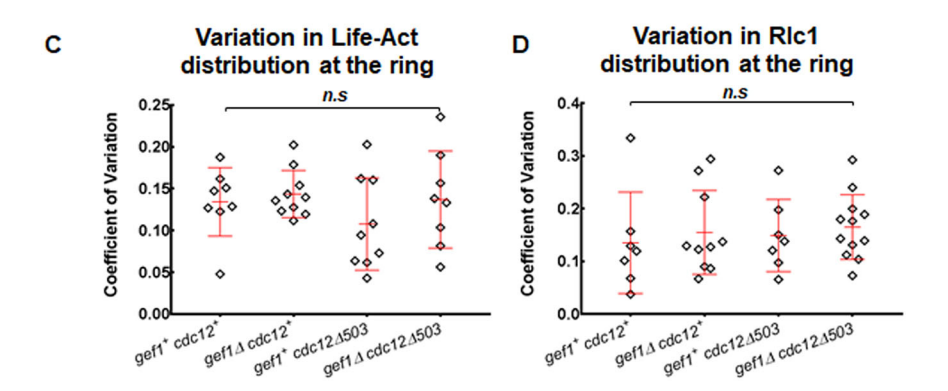


Fig. 3. Actin and myosin in the rings appear normal in mutants displaying non-concentric furrow formation. (A) 3D projections of cells expressing LifeAct-3×mCherry in indicated rings. The middle panel shows cells rotated by an angle of 50°. The lower panel shows 3D-reconstructed rings labeled with LifeAct-3×mCherry in the indicated strains. (B) 3Dreconstructed rings labeled with type II myosin light chain Rlc1-tdTomato in the strains as indicated. (C) Quantification of the CV of LifeAct-3×mCherry distribution along the ring in the indicated strains [n=9]; n.s., not statistically significant; one-way ANOVA (F(3,31)=1.058, P=0.381), with Tukey's multiple comparisons post hoc test]. (D). Quantification of the CV of Rlc1-tdTomato distribution along the ring in the indicated strains. [ $n \ge 7$ ; n.s., not statistically significant; one-way ANOVA (F(3,32)=0.2401, P=0.8677) with Tukey's multiple comparisons post hoc test]. Error bars represent standard deviation. Scale bars: 5 µm (cells); 2 µm (rings).



rapidly with the cytoplasmic pool, as per fluorescence recovery after photo bleaching (FRAP) experiments (Laporte et al., 2011; Roberts-Galbraith et al., 2010). To understand how Cdc15–GFP is distributed along the ring, we first investigated its dynamics at the actomyosin ring. We performed FRAP of Cdc15–GFP at rings during maturation in  $gef1^+cdc12^+$ ,  $gef1\Delta$ ,  $cdc12\Delta503$  and  $gef1\Delta cdc12\Delta503$  cells (Fig. 4A). While we did not see any change in the total recovery of Cdc15–GFP in the cells (Fig. 4A) the recovery was slower in  $gef1\Delta cdc12\Delta503$  cells as compared to  $gef1^+cdc12^+$  cells (Fig. 4A,B). The mean  $t_{1/2}$  of recovery was 17 s for  $gef1^+cdc12^+$ , 16 s for  $gef1\Delta$ , 24 s for  $cdc12\Delta503$  and 30 s for  $gef1\Delta cdc12\Delta503$  (Fig. 4B). A decrease in  $t_{1/2}$  occurs due to slower recovery of Cdc15–GFP to the ring after assembly in  $gef1\Delta cdc12\Delta503$  cells, compared to  $gef1^+cdc12^+$  cells.

We next enquired whether Cdc15 levels are lower in  $gef1\Delta cdc12\Delta 503$  mutants. To assess this, we compared the intensity of Cdc15–GFP along the ring during maturation in  $cdc12\Delta 503$  and  $gef1\Delta cdc12\Delta 503$  cells to that of  $gef1^+cdc12^+$  and  $gef1\Delta$  cells. Cells in anaphase B have rings in the maturation phase and are about to begin constriction (Wei et al., 2017; Wu et al., 2003). Cdc15–GFP intensity was measured in the rings of cells during anaphase B as determined by the distance between the spindle pole bodies marked with Sad1–mCherry (Fig. 4C). We find that Cdc15–GFP fluorescence intensity at the ring during anaphase B in  $gef1\Delta$  mutants is similar to that in  $gef1^+cdc12^+$  cells while it is

decreased in  $cdc12\Delta503$  cells by ~37% and in  $gef1\Delta cdc12\Delta503$  cells by ~34% cells (Fig. 4C,D). We verified that  $cdc12\Delta503$  and  $gef1\Delta cdc12\Delta503$  mutants did not show any decrease in overall protein levels in the cell by western blot analysis of total Cdc15–GFP (Fig. S2C,D). This suggested that, after ring assembly, Cdc15–GFP recruitment to the ring is impaired in  $cdc12\Delta503$  and  $gef1\Delta cdc12\Delta503$  cells. To further verify this, we analyzed the temporal fold increase in Cdc15-GFP levels in rings from the onset of maturation to the onset of constriction (Fig. 4E). We find that  $gef1^+cdc12^+$  and  $gef1\Delta$  cells show a 4- to 5-fold increase in Cdc15–GFP levels over time, while  $cdc12\Delta503$  and  $gef1\Delta cdc12\Delta503$  cells only show a 2-fold increase (Fig. 4E).

## Cdc15 recruitment to the assembled actomyosin ring requires the Arp2/3 complex

How Cdc15 is recruited to the assembled actomyosin ring after assembly remains unclear. We find that in the activated formin mutant, Cdc15 localization to the ring is impaired. As reported earlier and shown above, the activated formin mutants display a disorganized actin cytoskeleton (Fig. 1A,B, Fig. S1A; Coffman et al., 2013). Thus, we asked whether Cdc15 localization to the ring during maturation is actin dependent. Previous reports have shown that Cdc15 localizes to endocytic patches at the cortex and is involved in endocytosis (Arasada and Pollard, 2011; Carnahan and Gould, 2003; Balasubramanian et al., 1998; Chang et al., 1996).

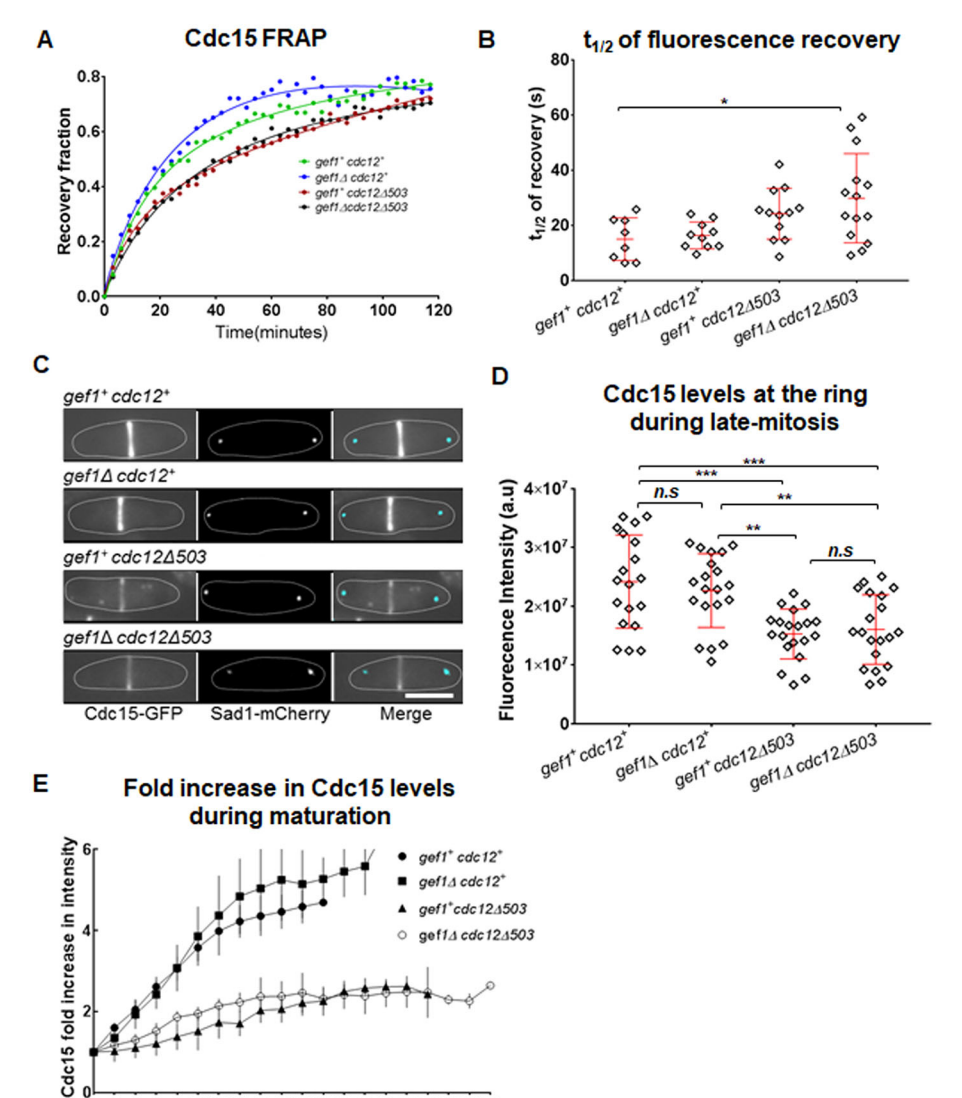


## Fig. 4. Activated *cdc12* mutants display reduced Cdc15 levels in the ring.

(A) Quantification of fluorescence recovery after photobleaching (FRAP) of Cdc15-GFP at the ring during maturation in the indicated strains. (B) Quantification of the  $t_{1/2}$  of FRAP of Cdc15– GFP in the indicated strains  $[n \ge 9 \text{ cells}; *P \le 0.05;$ one-way ANOVA (F(3,41)=3.667, P=0.0198) with Dunnett's multiple comparisons test]. (C) Sum projections of cells expressing Cdc15-GFP in late mitosis. The spindle pole bodies are labeled with Sad1-mCherry. (D) Quantification of fluorescence intensity of Cdc15-GFP at the actomyosin ring in the indicated strains [n=20 cells; \*\* $P \le 0.01$ ; \*\*\*P < 0.001; n.s., not statistically significant; oneway ANOVA (F(3,75)=10.52, P<0.0001) with Tukey's multiple comparisons post hoc test]. (E) Quantification of fold increase in Cdc15 levels during maturation in the indicated strains. Error bars represent standard deviation. Scale bar: 5 µm.

Endocytosis at the cell division site initiates during maturation after actomyosin ring assembly (Wang et al., 2016). Could Cdc15 be recruited during maturation to the division site via endocytic patches? Endocytic patches require the actin nucleator Arp2/3 complex that forms branched actin filaments (McCollum et al., 1996; Mullins et al., 1998, 1997; Welch et al., 1997; Winter et al., 1997). To test whether Cdc15 recruitment is affected by endocytosis, we treated cells expressing Cdc15-GFP with the Arp2/3 complex inhibitor CK666. CK666 treatment disrupted endocytic patches, as determined by the loss of LifeAct-3×mCherry- or Cdc15-GFP-labeled patches in cells (Fig. 5A, Fig. S3A). CK666 treatment did not block the assembly of Rlc1– tdTomato-labeled actomyosin rings or Cdc15-GFP recruitment to the ring during assembly (Fig. 5B,G). In DMSO-treated control cells, Cdc15 intensity increased after ring assembly by ~4-fold over a 10-min period, similar to what was found in previous reports (Fig. 5C,D; Wu and Pollard, 2005). However, after assembly, the ring in CK666-treated cells did not show any increase in Cdc15-GFP intensity (Fig. 5C,D). To verify that loss of Cdc15 recruitment to the ring after assembly is due to loss of Arp2/3 complex-mediated actin nucleation, we investigated Cdc15-GFP levels in arp3-c1

8 10 12 14 16 18 20 22 24 26 28 30 32 34 36 38

Time(minutes)

6

cold-sensitive mutants (McCollum et al., 1996). We find that in  $arp3^+$  cells and in arp3-c1 cells under permissive conditions, Cdc15–GFP levels after ring assembly show a ~4-fold increase over a 10-min period while arp3-c1 mutants at 20°C showed only a ~1.5-fold increase (Fig. 5E,F; Fig. S3B). These data suggest that Cdc15 recruitment to the ring depends on two independent mechanisms. During ring assembly, Cdc15 is recruited via precursor nodes (Laporte et al., 2011). After ring assembly, localization of Cdc15 to the actomyosin ring depends on the Arp2/3 complex, conceivably via endocytosis.

Cdc15 promotes cytokinetic events after ring assembly, such as ring stabilization and septum ingression (Arasada and Pollard, 2014; Cortés et al., 2015; Roberts-Galbraith et al., 2009; Wachtler et al., 2006). Temperature-sensitive *cdc15* mutants do not form a septum under restrictive conditions, and *cdc15* mutants lacking the SH3 domain show delays in the localization of the septum-synthesizing enzyme Bgs1 (Arasada and Pollard, 2014; Cortés et al., 2015). In agreement with the fact that Cdc15 levels during maturation did not increase in CK666-treated cells (Fig. 5C), we find that under these conditions onset of ring constriction and septum ingression was also inhibited (Fig. 5G). CK666-treated cells

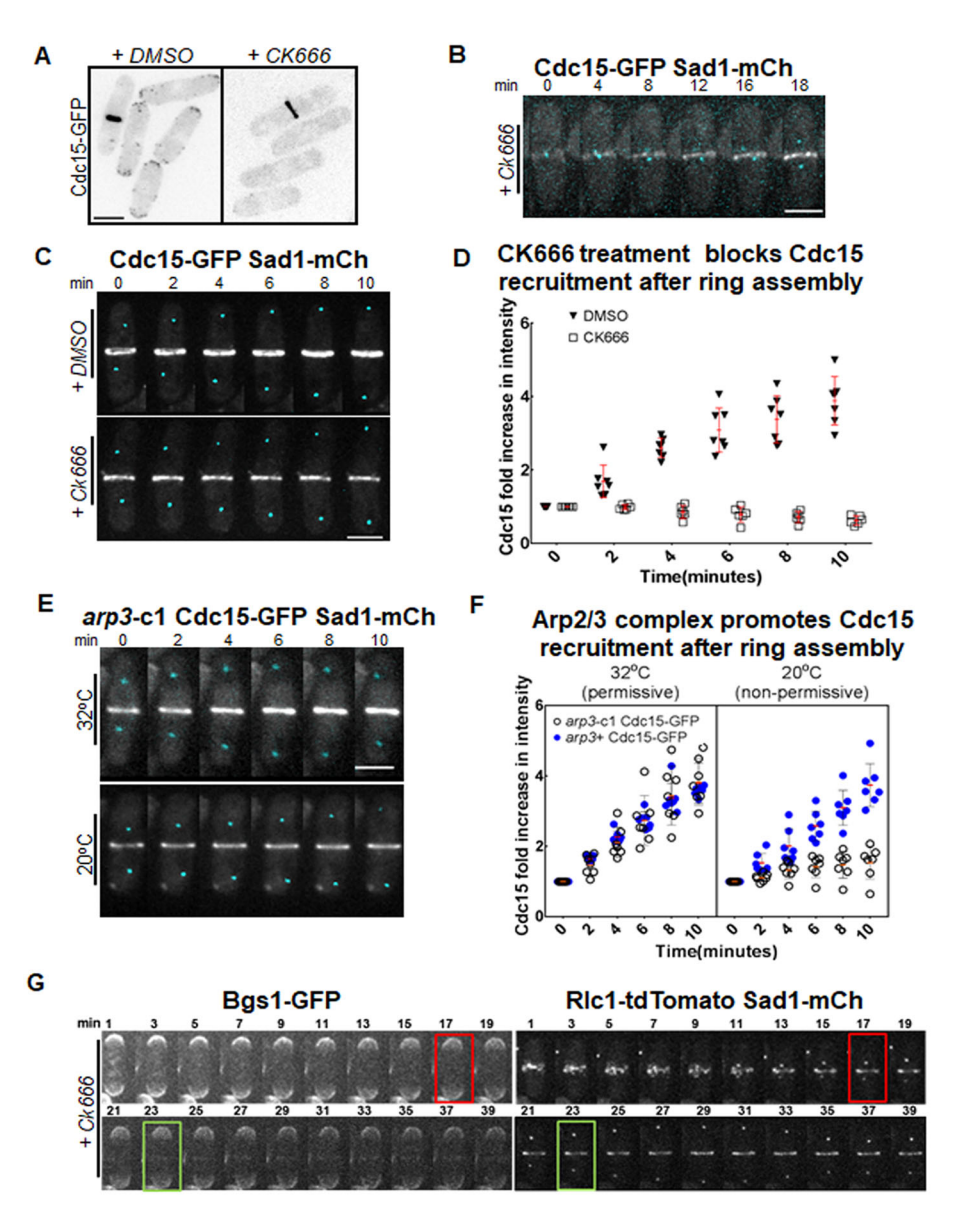


Fig. 5. Cdc15 recruitment to the assembled actomyosin ring requires the Arp2/3 complex. (A) Cdc15-GFP-labeled cortical patches in cells treated with DMSO or 100 µM CK666 for 5 min. (B) Time-lapse images showing Cdc15-GFP recruitment during ring assembly in cells treated with 100 µM CK666. Spindle pole bodies are labeled with Sad1-mCherry. (C) Time-lapse images of assembled rings in cells expressing Cdc15–GFP treated with DMSO or 100  $\mu M$ CK666. Spindle pole bodies are labeled with Sad1-mCherry. (D) Quantification of fold increase in Cdc15-GFP intensities over a 10-min time interval in cells treated with DMSO treated or 100 μM CK666 (*n*≥7 cells). (E) Time-lapse images of arp3-c1 cells expressing Cdc15-GFP and Sad1-mCherry after ring assembly. Time-lapse images of the control cells are shown in Fig. S2B. (F) Quantification of Cdc15-GFP fold increase in arp3+ and the arp3-c1 mutant, at permissive and non-permissive temperatures (n>7 cells). (G) Time-lapse images of 100 µM CK666-treated cells expressing Bgs1-GFP, Rlc1-tdTomato and Sad1-mCherry during ring assembly and maturation. The red box indicates an assembled actomyosin ring, the green box indicates when Bgs1-GFP first appears at the ring. Error bars represent standard deviation. Scale bars: 5 µm.

were able to assemble an actomyosin ring as shown by analysis of Rlc1-tdTomato, but failed to recruit Bgs1-GFP (Fig. 5G). In these cells, we observed an initial faint signal of Bgs1-GFP (Fig. 5E, green box) after ring assembly, but the intensity of this signal did not increase with time and the rings did not constrict (Fig. 5G). Cells that had already recruited Bgs1 to the ring and initiated constriction prior to treatment were able to complete the process (Fig. S3C). CK666 treatment also inhibited cell separation at the end of cytokinesis (Fig. S2D). Thus, after ring assembly, Arp2/3 complex-dependent events contribute to ring constriction and septum ingression, likely through localization of Cdc15 and Bgs1 to the division site.

## Cdc15 cortical patch dynamics are impaired in *gef1* and activated formin mutants

Since Cdc15 recruitment to the assembled ring requires the Arp2/3 complex, we asked whether endocytic events are disrupted in  $gef1\Delta cdc12\Delta 503$  mutants. We investigated Cdc15 localization at the endocytic patches in  $gef1\Delta cdc12\Delta 503$  mutants. Since Cdc15 is a highly abundant protein in the cell (Wu and Pollard, 2005), under

our experimental conditions, we were unable to distinguish Cdc15–GFP patches at the division site from proteins organized within the ring. To overcome this problem, we analyzed Cdc15–GFP patches at the cell tips during interphase. We find that cortical patches in  $gef1\Delta$ ,  $cdc12\Delta503$  mutants exhibit higher Cdc15-GFP intensity over time compared to  $gef1^+cdc12^+$  cells (Fig. 6A,B). In the double-mutant  $gef1\Delta cdc12\Delta503$ , Cdc15–GFP levels in the patch are further increased (Fig. 6A,B). In addition, the lifetime of Cdc15–GFP in cortical patches was longer in  $gef1\Delta$  and  $cdc12\Delta503$  mutants as compared to  $gef1^+cdc12^+$  cells, and further prolonged in  $gef1\Delta cdc12\Delta503$  double mutants (Fig. 6C). Taken together, these data indicate that Cdc15 patch dynamics are disrupted in  $gef1\Delta$  and  $cdc12\Delta503$  cells and that this defect is further aggravated in  $gef1\Delta cdc12\Delta503$  mutants.

To test whether Gef1 regulates patch dynamics through Cdc42 activation, we investigated Cdc15 patch dynamics in cells expressing the constitutively active Cdc42G12V. We expressed the constitutively active allele, cdc42G12V, under a mediumstrength thiamine-repressible promoter, nmt41, in  $gef1^+$  and  $gef1\Delta$  cells. Under moderate expression levels, cdc42G12V rescues the

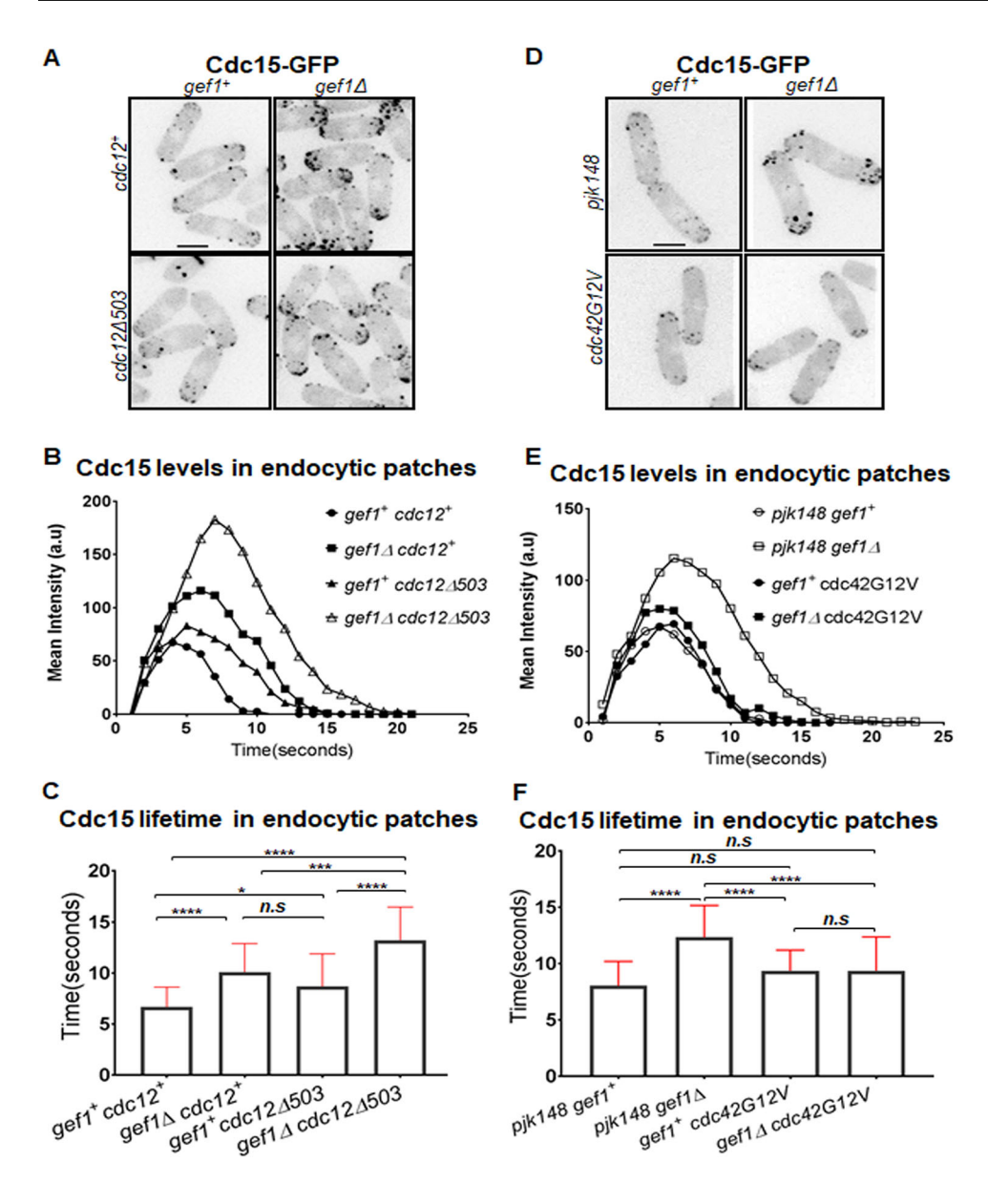


Fig. 6. Cdc15 cortical patch dynamics are impaired in gef1 and activated formin mutants. (A) Cdc15-GFP-labeled cortical patches in indicated strains. (B) Quantification of Cdc15-GFP levels over time in endocytic patches in strains indicated. (C) Quantification of Cdc15-GFP lifetimes at endocytic patches in the indicated strains [n=30 patches; \*P≤0.05; \*\*\*P < 0.001; \*\*\*\*P < 0.0001; n.s., not statistically significant; one-way ANOVA, (F(3,116)=28.34, P<0.0001) with Tukey's multiple comparisons post hoc test]. (D) Cdc15-GFP-labeled cortical patches in gef1<sup>+</sup> and gef1∆ cells, transformed with the empty vector pJK148, or expressing constitutively active cdc42G12V. (E) Quantification of Cdc15-GFP levels over time in endocytic patches in indicated strains. (F) Quantification of Cdc15-GFP lifetimes at endocytic patches in strains indicated [*n*=30 patches; \*\*\*\**P*≤0.0001; *n.s.*, not statistically significant; one-way ANOVA (F(3,116)=15.89, P<0.0001) with Tukey's multiple comparisons post hoc test]. Error bars represent standard deviation. Scale bars: 5 um.

delay in onset of ring constriction in  $gef1\Delta$  cells (Wei et al., 2016). Here,  $gef1^+$  and  $gef1\Delta$  cells bearing the empty pjk148 vector serve as experimental controls. In  $gef1\Delta$  cells expressing moderate levels of cdc42G12V, Cdc15–GFP intensity at the cortical patches is restored to levels observed in  $gef1^+$  cells bearing the control vector or expressing cdc42G12V (Fig. 6D,E). In agreement with this, the lifetime of Cdc15–GFP patches in  $gef1\Delta$  cells expressing moderate levels of cdc42G12V was restored to that observed in  $gef1^+$  cells bearing the control vector or expressing cdc42G12V (Fig. 6F). Thus, expression of cdc42G12V rescues the defects in Cdc15 patch intensity and dynamics in  $gef1\Delta$  mutants. These data indicate that Gef1 contributes to Cdc15 levels and dynamics in the patches through Cdc42 activation.

## Model to define uniform protein distribution along the ring-membrane interface

Our data show non-concentric furrowing in cells that display irregular Cdc15 distribution along the ring during maturation. To explore potential mechanisms governing how Cdc15 is recruited and distributed at the actomyosin ring during maturation, we developed

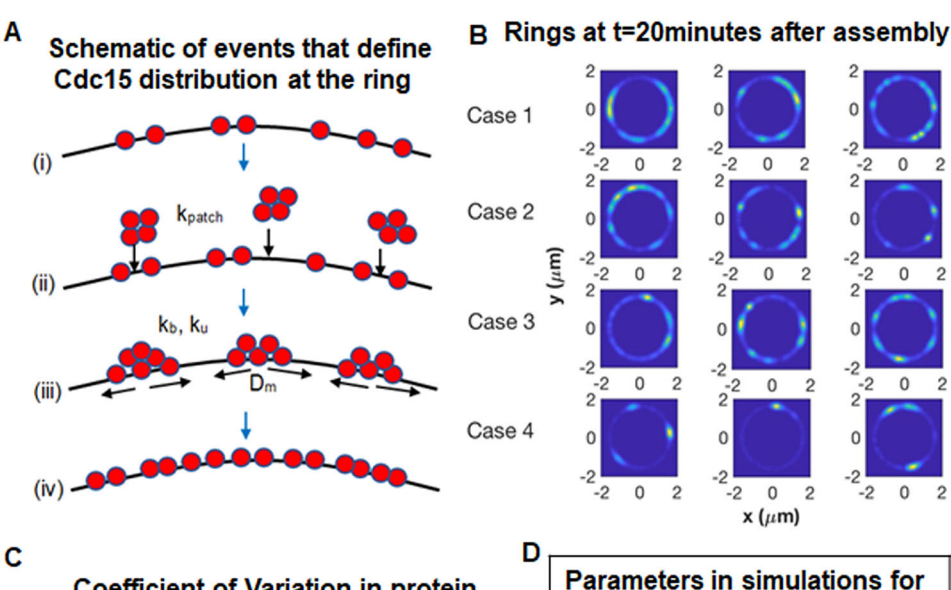
a mathematical model. We find that Arp2/3-mediated actin nucleation is required for Cdc15 recruitment to the actomyosin ring after assembly. Furthermore,  $gef1\Delta cdc12\Delta 503$  cells display irregular Cdc15 distribution along the ring and non-concentric furrow formation. Cdc15 is recruited to endocytic patches immediately after initiation of actin nucleation (Arasada and Pollard, 2011) and its intensity increases as the patch size increases. However, Cdc15 does not internalize with the endocytic patch, but rather appears to dissipate from the cortex by an unknown mechanism (Arasada and Pollard, 2011). As is evident from the nano-scale structure of the cytokinetic ring, Cdc15 associates with the membrane adjacent to the ring through the membrane-binding BAR domain (McDonald et al., 2017, 2015). Our model posits that when endocytic patches at the plasma membrane next to the ring are internalized, Cdc15 molecules associated with the patches do not dissipate into the cytoplasm, but instead associate with the proteins at the ring-membrane interface. Thus, Cdc15 levels at the division site increase as endocytosis continues.

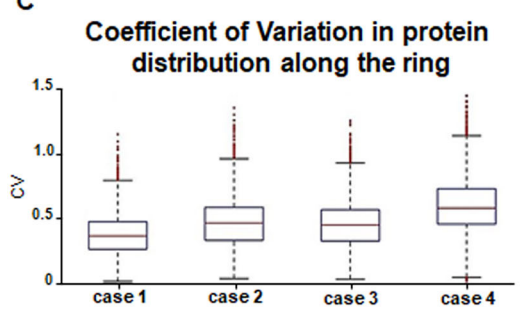
In the mathematical model, we define biophysical rules for the behavior of Cdc15, and characterize its spatial distribution as a function of time during ring maturation (Fig. 7A). The model is stochastic in nature and considers the behavior of individual Cdc15 proteins. The proteins can diffuse on the ring and associate with other Cdc15 molecules to form clusters, which we assume have a small diffusion coefficient and are effectively immobile. The population of Cdc15 increases over time due to recruitment from endocytic patches. Because Cdc15 proteins associated with an endocytic patch are spatially localized, they are recruited to the ring in a spatially correlated manner. Thus, if only a few, but large, patches of Cdc15 are recruited and are effectively immobile due to a small diffusion coefficient, this can result in irregular protein distribution.

The model is parameterized by the rate at which endocytic patches are internalized near the ring ( $k_{\text{patch}}$ ), the number of Cdc15 molecules per patch  $(N_{\text{patch}})$ , the total number of proteins in the ring at the end of maturation  $(N_{\text{total}})$ , the diffusion coefficient of Cdc15 on the ring  $(D_{\rm m})$ , and the rates of binding to  $(k_{\rm b})$  and unbinding from  $(k_{\rm u})$  clusters. Details of the model can be found in the Materials and Methods. We investigated different sets of parameters representing our experimental observations in  $gef1^+cdc12^+$ ,  $gef1\Delta$ ,  $cdc12\Delta503$  and  $gef1\Delta cdc12\Delta 503$  cells (cases 1–4, respectively, Fig. S4). For each set, we performed computer simulations to generate multiple independent trajectories, each of which represents the spatiotemporal evolution of Cdc15 in the ring of a single cell. Fig. 7B shows snapshots from simulations depicting the spatial distribution of Cdc15 on the ring for different genotypes (cases). We find that the Cdc15 distribution in our simulated rings was approximately uniform for cases 1-3, which represent  $gef1^+cdc12^+$ ,  $gef1\Delta$  and  $cdc12\Delta503$  cells. However, case 4, representing  $gef1\Delta cdc12\Delta 503$  cells, showed the most irregular Cdc15 distribution (Fig. 7B). We further verified this by measuring the CV for 10,000 simulated rings for each case (Fig. 7C). We find that case 1, simulating  $gef1^+cdc12^+$  conditions, has the lowest median CV and case 4, simulating  $gef1\Delta cdc12\Delta 503$  conditions, has the largest median value, with the distribution most prominently shifted toward larger values of CV. Because of the large number of simulations, differences between all distributions are statistically significant. Our simulations reveal that, similar to experimental observations in  $gef1\Delta cdc12\Delta 503$  cells, Cdc15 distribution along the ring is most irregular under conditions in which the number of molecules in each patch is increased and the rate of patch association is decreased. Thus, our model indicates that the distribution of Cdc15 along the ring is impacted by the patch association rate and the number of molecules in each patch.

#### **DISCUSSION**

In fission yeast, coordination of ring constriction and septum ingression leads to concentric furrow formation. Here, we report that the *gef1\Deltacl2\Delta503* mutant displays non-concentric furrow formation and an irregular rate of constriction along the ring, suggesting a disruption in the coordination of these processes. These mutants display uneven distribution of the F-BAR protein Cdc15 at the ring, and sections of the ring exhibiting higher Cdc15 levels undergo faster constriction. Previous reports show that Cdc15 is a ring component that promotes septum ingression (Roberts-Galbraith et al., 2009). Defining what determines uniform Cdc15 distribution along the ring will provide insights into how ring





| modelling Cdc15 distribution along the ring |   |
|---|---|
| Ring Circumference                          | 10 µm                                     |
| Binding rate, k <sub>b</sub>                | 10 min <sup>-1</sup>                      |
| Unbinding rate, K <sub>u</sub>              | 1 min <sup>-1</sup>                       |
| Diffusion coefficient, $D_m$                | 0.02 µm <sup>2</sup><br>min <sup>-1</sup> |
| Initial amount of protein, $N_0$            | 500                                       |

Fig. 7. A mathematical model defines Cdc15 protein distribution along the ring during cytokinesis. (A) Schematic of model (from top down): (i) a small initial population of Cdc15 proteins (red) are randomly distributed on the ring; (ii) patches of Cdc15 proteins (from endocytic patches) associate to random locations on the ring at rate  $k_{patch}$ ; (iii) proteins can bind to (rate  $k_{\rm b}$ ) and unbind from (rate  $k_{II}$ ) each other and diffuse along the ring with diffusion coefficient  $D_{\rm m}$ ; (iv) as time progresses, proteins accumulate and become distributed along the ring. (B) The spatial distribution of Cdc15 along the ring at t=20 min. Three independent simulated rings are shown for each of the four simulated cases. (C) Box plots of the CV for 10,000 simulations of each of the four simulated cases. For each box, the central (red) mark is the median, the edges of the box are the 25th and 75th percentiles, and the whiskers extend to the most extreme data points not considered outliers. Outliers are plotted individually. The differences between all pairs of cases are significant with P-values all below 4×10<sup>-5</sup>. (D) Parameter values used in all ring simulations. The number of proteins was obtained from previously published work (Wu and Pollard, 2005).

constriction and septum ingression are coordinated. Our data indicate that after ring assembly, the Cdc42 GEF Gef1 and endocytic events promote uniform Cdc15 organization at the ring.

While the rings in cells displaying non-concentric furrow formation show irregular Cdc15 distribution, they did not show any defects in F-actin organization or type II myosin distribution. This suggests that although the assembled rings themselves are spatially uniform, Cdc15 localization is not. This further indicates that factors apart from those involved in ring assembly, determine how proteins are organized along the ring. To understand how Cdc15 is distributed along the ring, we first investigated how it is recruited to the actomyosin ring. Cdc15 is initially recruited to the division site via precursor nodes (Laporte et al., 2011; Wu et al., 2003, 2006). After ring assembly, Cdc15 levels at the ring increases until the onset of constriction (Wu and Pollard, 2005). We find that the increase in Cdc15 levels after ring assembly is dependent on Arp2/3 complex-dependent actin patch formation. Disruption of the Arp2/3 complex in hypomorphic mutants or by CK666 treatment did not affect Cdc15 recruitment to the precursor nodes, but eliminated any increase in levels after ring assembly. This indicates that Cdc15 is recruited to the division site during ring assembly and maturation by two different mechanisms, with the Arp2/3 complex being required during maturation. Moreover, we found that inhibition of Arp2/3 complex activity inhibited Bgs1 localization to the division site as well as the onset of ring constriction. In cells in which Bgs1 was delivered to the division site prior to inhibitor treatment, the rings were able to constrict. Endocytosis and exocytosis are coupled processes, and inhibiting one process could lead to disruption of the other. It is possible that blocking endocytosis leads to disruption of exocytosis and thus delivery of Cdc15 to the division site. Indeed, it has been suggested that Cdc15 may facilitate Bgs1 delivery from the Golgi complex (Arasada and Pollard, 2014). However, while Cdc15-GFP is readily visible in endocytic patches and at the actomyosin ring, we did not see any Cdc15 localization at the secretory vesicles or the Golgi. Moreover, Cdc15 is not required for the localization of the Golgi to the division site (Vjestica et al., 2008). We find that Cdc15 localization to the endocytic patches is lost during CK666 treatment and in arp3 mutants. Previous reports have shown that, during endocytic patch internalization, Cdc15 in the patch itself does not internalize but is instead lost from it (Arasada and Pollard, 2011). High-resolution microscopy shows that the Cdc15 BAR domain associates with the membrane while the scaffold SH3 domain extends into the ring (McDonald et al., 2017). At the membrane, Cdc15, via its BAR domain, also associates with Cdc12. However, cdc12 mutants unable to interact with Cdc15 do not display any ring constriction defects (Willet et al., 2015). This suggests that while Cdc15 contributes to Cdc12 localization, the reciprocal relationship does not exist. Based on our data we postulate that, at the division site, when the endocytic patches that overlap with the actomyosin ring internalize, the Cdc15 from the patch is incorporated into the ringmembrane interface.

We find that the fold-increase in Cdc15 levels during ring maturation is reduced in  $cdc12\Delta503$  and  $gef1\Delta cdc12\Delta503$  mutants. Our data suggest that the activated formin mutant influences Cdc15 localization to the ring. We posit that low levels of Cdc15 at the ring contribute to its irregular distribution and subsequent nonconcentric furrow formation. Previous reports as well as our own findings have shown that  $cdc12\Delta503$  (Coffman et al., 2013) and  $gef1\Delta cdc12\Delta503$  mutants display an increased number of actin cables. An increase in actin cable formation leads to defects in endocytosis due to disruption of actin homeostasis and increased

competition for actin monomers (Gao and Bretscher, 2008; Suarez et al., 2015). While we did not see any decrease in actin patch formation in activated formin mutants, we did observe prolonged Cdc15 patch lifetimes at the cortex. Thus, it is possible that actin homeostasis is disrupted in the activated formin mutant, leading to defects in endocytic patch dynamics and therefore reduced Cdc15 levels at the ring.

While the rings in both  $cdc12\Delta503$  and  $gef1\Delta cdc12\Delta503$  mutants display decreased levels of Cdc15, only gef1Δcdc12Δ503 mutant rings display irregular Cdc15 distribution and non-concentric furrow formation. This reveals a role for Gefl in Cdc15 distribution along the ring. We show that Gef1 limits the levels of Cdc15 in individual endocytic patches at the cortex. Both  $gef1\Delta$  and  $gef1\Delta cdc12\Delta 503$  mutants show increased Cdc15 levels over time at cortical endocytic patches. Cdc15 recruitment to the patch stops once internalization initiates during endocytosis (Arasada and Pollard, 2011). We find that patch lifetime in  $gefl\Delta$  and  $gef1\Delta cdc12\Delta 503$  mutants is prolonged. It is possible that patch internalization is delayed in these mutants, thereby prolonging Cdc15 recruitment and increasing its levels in patches. Cdc15 levels in the patches and the patch lifetimes can be restored to normal by expression of constitutively active Cdc42 in gef1\Delta mutants. The downstream targets of Cdc42 that regulate endocytosis in fission yeast are not well defined. The Cdc42 target Pak1 kinase is an activator of the type I myosin Myo1 (Attanapola et al., 2009) and may contribute to the process. However, we find that in the hypomorphic pak mutant orb2-34, Cdc15 distribution at the ring was not impaired. This suggests that additional targets of Cdc42 may regulate endocytosis and Cdc15 recruitment.

Our data indicate that Gef1 plays an important role in actomyosin ring constriction when Cdc15 levels in the ring are compromised due to  $cdc12\Delta503$  mutation. The activated  $cdc12\Delta503$  allele can restore non-medial actin cables in  $gefl\Delta$  cells. However, this does not rescue the defect in the onset of ring constriction observed in *gef1* mutants. Instead, the endocytic defects in cdc12Δ503 mutants are exacerbated in  $gefl\Delta$  mutants displaying slower endocytic patch dynamics, increased Cdc15 levels in the patches, and non-concentric constriction. Our data indicate that Cdc15 distribution along the ring is irregular under conditions in which Cdc15 displays slower dynamics at the ring and increased levels in individual cortical patches. We propose a model to explain how Cdc15 is organized at the ring after assembly and under what conditions this organization is disrupted. In our model, Cdc15 is incorporated into the ring from endocytic patches when endocytosis is initiated at the membrane overlapping the actomyosin ring. Since Cdc15 remains in the patches until internalization, it is possible that its incorporation from the patches can be delayed if patch internalization itself is delayed. In addition, the amount of Cdc15 incorporated from each endocytic patch also influences its distribution. Under conditions where the number of molecules in each patch is high and the rate of patch incorporation is slow, Cdc15 distributes irregularly at the ring. This suggests that the rate of endocytosis at the division site and the protein quantity in these patches together determine how Cdc15 is spatially distributed at the ring.

Previous reports suggest that Cdc15 has a role in actomyosin ring assembly (Carnahan and Gould, 2003; Chang et al., 1996; Fankhauser et al., 1995). However, inhibition of *cdc15* expression or deletion of its scaffolding SH3 domain did not result in any actomyosin ring formation defects (Arasada and Pollard, 2014; Roberts-Galbraith et al., 2009). While *cdc15* is not required for actomyosin ring formation during early stages of cytokinesis, it is necessary for cytokinetic events after metaphase (Wachtler et al.,

2006). In anillin *mid1* mutants, ring formation depends on SIN pathway-mediated phospho-regulation of Cdc15 (Hachet and Simanis, 2008; Wachtler et al., 2006). Recent reports indicate that Cdc15 plays a more important role during ring maturation and constriction (Arasada and Pollard, 2014; Ren et al., 2015; Roberts-Galbraith et al., 2010). How does uniform Cdc15 distribution ensure concentric furrow formation? In both gef1 and cdc15 mutants, Bgs1 localization is delayed at the ring with a corresponding delay in onset of furrow formation (Arasada and Pollard, 2014; Cortés et al., 2015; Wei et al., 2016). It is possible that Gef1 regulates Cdc15 organization via Cdc42 activation to ensure timely Bgs1 localization and onset of furrow formation. The SH3 domain of Cdc15 acts as a scaffold that binds several proteins and maintains them at the ring (Cortés et al., 2015; McDonald et al., 2017; Ren et al., 2015; Roberts-Galbraith et al., 2009). This includes the GTPase Rho1 GEF, Rgf3 (Ren et al., 2015). Details of how Cdc15 promotes septum ingression remain unclear. One potential mechanism could be through the localization of Rgf3 that activates Rho1, the regulatory subunit for glucan synthases such as Bgs1 and Bgs4 (Arellano et al., 1996; Morrell-Falvey et al., 2005; Mutoh et al., 2005). In the absence of Cdc15 interaction, Rgf3 likely fails to localize and activate Rho1 at the ring and this in turn could fail to activate the glucan synthases. We postulate that sections of the ring with decreased Cdc15 do not properly activate the glucan synthases and thus display slower rates of ring constriction and septum ingression. Proper organization of Cdc15 along the ring is therefore important for uniform septum ingression in coordination with actomyosin ring constriction.

Actomyosin ring-based cytokinesis is observed mainly in animal and fungal cells, and the nature of furrow formation in these systems differs according to the cell type. Whereas in fungal cells cytokinesis involves coordination of actomyosin ring constriction and septum ingression, in animal cells, ring constriction is coordinated with membrane expansion (Prekeris and Gould, 2008). In certain animal cells, such as embryos and polarized epithelial cells, furrow formation occurs in a non-concentric manner (Maddox et al., 2007). This manner of constriction likely maintains cell-cell contacts in epithelial cells and supports rapid cell division during embryonic development (Dorn et al., 2016; Maddox et al., 2007). It has been reported that septin and anillin scaffold proteins are required for non-concentric furrowing (Maddox et al., 2007). A recent model indicates that a non-concentric furrow can form even in the absence of preexisting cues due to feedback between membrane curvature and cytoskeletal rearrangements (Dorn et al., 2016). Proper furrow formation in fission yeast has been described in a mathematical model that indicates that septum deposition is a mechanosensitive process and that actomyosin ring tension and curvature drive this process (Thiyagarajan et al., 2015). An impaired actomyosin ring results in irregular septum ingression and furrow formation. Our results provide mechanistic insights into how an assembled actomyosin ring acts as a landmark around which proteins are organized to promote septum ingression and furrow formation.

#### **MATERIALS AND METHODS**

#### Strains and cell culture

Strains used in this study are listed in Table S1. All *S. pombe* strains used in this study are isogenic to PN972. Unless otherwise noted, cells were cultured in yeast extract (YE) medium and grown exponentially at 25°C. Genetic manipulations of strains were carried out using standard techniques (Moreno et al., 1991). Cells were grown exponentially for at least three rounds of eight generations before each assay.

#### Microscopy

Image acquisition was performed at room temperature (23-25°C) with a VT-Hawk 2D array scanning confocal microscope (VisiTech Intl., Sunderland, UK) using an Olympus IX-83 inverted microscope with a 100×/numerical aperture 1.49 UAPO lens (Olympus, Tokyo, Japan). For still images, cells were mounted directly onto glass slides with a #1.5 coverslip (Fisher Scientific, Waltham, MA) and imaged promptly. For all z-series, images were acquired with a depth interval of 0.4 μm. In time-lapse image acquisition, cells were placed in a 3.5-mm glass-bottom culture dish and covered with YE medium with 0.6% agar. Ascorbic acid (100 µM vitamin C) was added to the cell culture to minimize fluorescence toxicity, as previously reported (Wei et al., 2017). Images were acquired with MetaMorph (Molecular Devices, Sunnyvale, CA). For the FRAP experiments, we used the SP8 confocal microscope with 63×1.4NA oil objective (Leica Microsystems). Images were acquired with the Leica Application Suite X software. All images were analyzed with ImageJ (National Institutes of Health, Bethesda, MD). Statistical analysis was performed using one-way ANOVA, followed by Tukey's honestly significant difference (HSD) post-hoc test or Dunnett's post-hoc tests where appropriate. Comparisons between experimental groups were considered significant when  $P \le 0.05$ .

#### **Phalloidin staining**

The actin cytoskeleton was stained as described previously (Das et al., 2009; Pelham and Chang, 2002). We fixed exponentially growing cells with 3.5% formaldehyde (Sigma-Aldrich) and incubated at room temperature (23–25°C) for 10 min. The fixed cells were washed with PM buffer (35 mM potassium phosphate pH 6.8, 0.5 mM MgSO<sub>4</sub>) and permeabilized with 1% Triton in PM buffer. Finally, cells were washed again in PM buffer and then stained with Alexa-Fluor–phalloidin at room temperature for 30–45 min. The number of actin cables was analyzed as described previously (Wei et al., 2016).

#### Calculating Cdc15 fraction intensity at the ring

Kymographs for rings in  $gef1\Delta cdc12\Delta 503$  mutants were obtained via ImageJ analysis of time-lapse movies. We first measured Cdc15 intensity at two edges of the ring on the kymographs at the onset of constriction (x and y). Cytoplasmic fluorescent signal was used for background subtraction. To determine the fraction intensity of Cdc15 at each edge/side of the ring (x and y), we divided the intensity of Cdc15 at that edge by the total sum of Cdc15 intensity at both edges. Hence, for edge x, the fraction of Cdc15 intensity is obtained using the formula x/(x+y), while the fraction intensity for edge y is calculated as y/(x+y).

#### **Counting medial actin patches**

Z-series image acquisition of phalloidin-stained cells was performed via confocal microscopy. With the exception of the cell tips, all patches in the middle region of interphase cells were counted (Fig. S1B). Counting of medial patches was performed in ImageJ via maximum z-projections, and by scrolling through each focal plane in the raw image.

#### **Quantification of Cdc15 levels**

Time-lapse movies of strains were obtained for a duration of 5 min, and image acquisition occurred every second for each movie. By using ImageJ, the appearance and disappearance of Cdc15–GFP in the patches at the tips of interphase cells was recorded. Patches were selected using a circular region of interest (ROI) of diameter 0.5 μm, as described previously (Berro and Lacy, 2018). Background subtraction was performed for each patch by measuring intensity in the cytosol using the same ROI size. The fold increase in intensity was calculated after background subtraction. A total of 30 patches for each strain was measured for this analysis.

To quantify Cdc15 levels in cells during late mitosis, we acquired *z*-series images of all strains. Sum projections of each image was obtained using ImageJ. Cells in late mitosis were identified by means of the position of and distance between the spindle pole bodies. The cytoplasmic fluorescent signal was used for background subtraction,

To measure the fold increase of Cdc15 during ring maturation, time-lapse movies were obtained for all strains. Sum projections of movies in ImageJ

were used for quantification and image analysis. Cdc15 levels at the ring were measured from the time the ring formed to the last time-point preceding constriction initiation. We measured Cdc15–GFP intensity at the ring over time by using an ROI to select the Cdc15–GFP signal at the division site. The cytosol of each cell was used to correct for background noise in that cell. Background subtraction was performed for each cell by measuring intensity in the cytosol using the same ROI size and subtracting this value from the signal, for each time point. The fold increase in intensity was calculated after background subtraction.

#### Imaging of arp3-c1 strains

The cold-sensitive mutant *arp3-c1* expressing Cdc15–GFP and Sad1–mCherry was grown in YE at 32°C and shifted to 19°C for 12 h as previously described (McCollum et al., 1996). The cells were imaged via time-lapse confocal imaging. Under our conditions the cells were imaged at 20°C.

#### Fluorescence recovery after photobleaching

Cells with an actomyosin ring in the maturation phase were first focused at the medial z-plane. At the medial plane, the Cdc15-GFP-labeled ring appears as two spots on either edge of the cell cortex. One such spot was marked as the ROI, and four images were acquired pre-bleach. The ROI was then bleached for 10 s and images were then acquired every 3 s for 50–100 images. The non-bleached spot for the same ring was also analyzed to account for loss of signal due to photobleaching over time. A cell-free region of the image was used for background subtraction. Intensity values for each ROI were corrected for loss of signal over time and background signal. The intensity values were then normalized against the mean pre-bleach value to determine the recovery fraction over time. At least ten rings were analyzed for each genotype. The average corrected and normalized intensity values were then plotted as fraction of recovery over time. The data were then fitted to a single-exponential curve of the functional form,  $f(x) = m_1 + m_2 e^{-m_3 x}$ , where  $m_3$  is the off rate and  $m_1$  is the plateau of recovery. The half-life  $(t_{1/2})$ was then computed as  $t_{1/2} = ln(2)/m_3$ . Biphasic recovery curves were then constructed using a double-exponential form of the curve-fitting function,  $f(x) = m_1 + m_2 e^{-m_3 x} + m_4 e^{-m_5 x}$ .

#### **CK666 treatment**

Cells were treated with  $100 \,\mu\text{M}$  CK666 (Sigma-Aldrich, SML006-5MG) in dimethyl sulfoxide (DMSO, Sigma-Aldrich, D8418-250ML). Control cells were treated with 0.1% DMSO in YE medium. For time-lapse images, the agar pads (Wei et al., 2017) were also treated with  $100 \,\mu\text{M}$  CK666 or DMSO.

#### **Expressing constitutively active Cdc42**

The cdc42G12V fragment was cloned into the pJK148 vector under the thiamine-repressible promoter nmt41 and integrated into the genome of gef1+ and  $gef1\Delta$  cells, as previously described in Wei et al. (2016). To ensure low expression levels of cdc42G12V, cells were grown in YE medium at 25°C. The experimental controls were gef1+ and  $gef1\Delta$  cells transformed with the empty pJK148 vector.

#### **Protein methods**

Cells growing exponentially were harvested by centrifuging at 2900 g for 5 min and washed with STOP buffer (150 ml of NaCl, 50 mM NaF, 10 mM EDTA, 1 mM NaN<sub>3</sub>, pH 8). Cells were lysed with 150  $\mu$ l RODEL mix (1.85 M NaOH, 1 M  $\beta$ -mercaptoethanol and 1 mM PMSF), 500  $\mu$ l water and 650  $\mu$ l of 50% trichloroacetic acid. The precipitate was incubated in ice for 30 min, centrifuged at 17,000 g for 10 min at 4°C, washed with 0.5 M Tris base (pH not adjusted) and finally washed with water. The pellet was then dissolved in gel-loading buffer. The samples were used for routine western blot analysis. Primary antibodies used were polyclonal anti-GFP (1:2000, Torrey Pines Biolabs, TP401, lot #081211), and monoclonal anti- $\alpha$ -tubulin (1:2000, Sigma-Aldrich, T6074, lot #034M4837). Conjugated anti-mouse IRDye 800 and anti-rabbit IRDye 680 antibodies were used as secondary antibodies (LI-COR Biosciences, 926-32210, lot #C50113-06; 926-68071, lot #C41217-03). The blots were then analyzed using the Odyssey Infrared Imaging system (LI-COR Biosciences).

## Modeling protein distribution along the ring via endocytic patch internalization

#### Calculating the number of Cdc15 proteins at the ring during maturation

The local concentration of Cdc15 at the actomyosin ring and endocytic patches was based on previous reports (Arasada and Pollard, 2011; Wu and Pollard, 2005). At the end of assembly, the ring contains  $\sim$ 500 molecules of Cdc15. During maturation, this number increases to  $\sim$ 2500 molecules at which time the ring starts to constrict. We used this information to assign  $\sim$ 2500 molecules of Cdc15 to mature rings in case 1 and 2, which mimic rings in  $gef1^+cdc12^+$  and  $gef1\Delta$  cells, respectively. Based on the percentage decrease in Cdc15 levels at the ring in  $cdc12\Delta503$  and  $gef1\Delta cdc12\Delta503$  mutants, we computed the number of Cdc15 molecules for case 3 and 4, respectively (Table S2). Table S2 represents protein concentrations at the rings used for all four strains in the model.

#### Calculating the number of Cdc15 molecules in individual patches

As per previous reports we assigned ~130 molecules of Cdc15 to each cortical patch (Arasada and Pollard, 2011) in case 1 mimicking  $gef1^+cdc12^+$  cells. For cases 2, 3 and 4, we computed the number of Cdc15 molecules in the patches based on the fold change in our intensity measurements in  $gef1\Delta$ ,  $cdc12\Delta503$  and  $gef1\Delta cdc12\Delta503$  mutants, respectively (Fig. S4B).

#### Defining parameters in the model

The mathematical model describes discrete-space continuous-time stochastic dynamics of Cdc15 proteins on a one-dimensional actomyosin ring. The ring is  $10~\mu m$  in length and is discretized into lattice sites of length  $0.1~\mu m$ . At the start of maturation, a relatively small number of Cdc15 proteins (500) are randomly distributed on the ring. The population then increases as endocytic patches near the ring are internalized, leaving groups of Cdc15 to associate with the ring. Once associated with the ring, Cdc15 proteins diffuse along the ring and can bind to other Cdc15 molecules. Multiple proteins are allowed to occupy a single lattice site.

 $N_{\rm patch}$  represents the average number of Cdc15 molecules per endocytic patch while  $N_{\rm total}$  is the average number of proteins on the ring at the end of maturation. The number of proteins that associate to the ring from a particular endocytic event is sampled from a normal (Gaussian) distribution with a mean  $N_{\rm patch}$  and standard deviation corresponding to the experimentally measured Cdc15 patch intensity distribution. The rate at which patches of Cdc15 associate with the ring ( $k_{\rm patch}$ ) is specified so that the average number of proteins after 20 min is  $N_{\rm total}$ . The parameters  $N_{\rm total}$  and  $N_{\rm patch}$  are varied to represent different cell genotypes.

Each patch of Cdc15 associates with a random location on the ring; all Cdc15 molecules from the patch are initially placed in the same lattice site. Once on the ring, proteins can diffuse or bind with each other to form clusters. Unbound proteins diffuse on the ring by hopping to nearest neighbor lattice sites at the rate  $k_{\text{hop}}$  specified by the diffusion coefficient  $(D_{\text{m}})$ . Proteins occupying the same lattice site can bind to form oligomers (with binding rate  $k_{\text{b}}$ =10 min<sup>-1</sup>). Cdc15 within oligomers can unbind to form mobile monomers (with unbinding rate  $k_{\text{u}}$ =1 min<sup>-1</sup>). We use the Gillespie algorithm to generate independent stochastic simulation trajectories. The propensity (rate) of each type of reaction is given by:

Association: 
$$a_1 = \begin{cases} k_{\text{patch}} & \text{if } N < N_{\text{total}} \\ 0 & \text{if } N \ge N_{\text{total}} \end{cases}$$
, (1)

Diffusion: 
$$a_2 = k_{\text{hop}} \sum_{i=1}^{n_{\text{sites}}} N_{\text{u}}(i),$$
 (2)

Binding: 
$$a_3 = k_b \sum_{i=1}^{n_{\text{sites}}} max\{[N_{\text{u}}(i) - 1], 0\},$$
 (3)

Unbinding: 
$$a_4 = k_u \sum_{i=1}^{n_{\text{sites}}} \max\{[N_b(i) - 1], 0\}.$$
 (4)

Here, N is the number of Cdc15 molecules on the ring,  $n_{\text{sites}}$  is the total number of lattice sites, and  $N_{\text{u}}(i)$  and  $N_{\text{b}}(i)$  represents the number of unbound and bound proteins in site i, respectively. The propensity of binding,  $a_3$ , is the product of the binding rate constant  $k_{\text{b}}$  and the number of potential bonds in the system (Eqn 3) while the propensity of unbinding,  $a_4$ , is the product of

the unbinding rate constant  $k_{\rm u}$  and the number of bonds in the system (Eqn 4). We have conducted simulations for diffusion coefficients spanning multiple orders of magnitude (0.002 to 20  $\mu {\rm m}^2/{\rm min}$ ). We observe similar results across the range of  $D_{\rm m}$  when the binding rate ( $k_{\rm b}$ ) increases with  $D_{\rm m}$ .

#### Acknowledgements

We thank B. McKee, B. Hercyk and J. Rich for critically reviewing our manuscript; and J. Q. Wu, K. Gould and P. Perez for providing strains.

#### Competing interests

The authors declare no competing or financial interests.

#### **Author contributions**

Conceptualization: S.M.A., M.E.D.; Methodology: U.N.O., P.J.M., B.W.; Validation: U.N.O.; Formal analysis: U.N.O., P.J.M., B.W., S.M.A., M.E.D.; Investigation: U.N.O., P.J.M., B.W., J.H., A.C., M.E.D.; Resources: M.E.D.; Data curation: U.N.O., P.J.M., B.W., M.E.D.; Writing - original draft: U.N.O., M.E.D.; Writing - review & editing: U.N.O., P.J.M., S.M.A., M.E.D.; Supervision: S.M.A., M.E.D.; Project administration: M.E.D.; Funding acquisition: M.E.D.

#### **Funding**

This work is supported by the National Science Foundation (1616495) and TN-SCORE, a multi-disciplinary research program sponsored by National Science Foundation EPSCoR (EPS-1004083). U.N.O. was supported by National Institutes of Health (IMSD) (R25GM086761) and is currently supported by a National Science Foundation Graduate Research Fellowship (DGE-1452154). Deposited in PMC for release after 12 months.

#### Supplementary information

Supplementary information available online at http://jcs.biologists.org/lookup/doi/10.1242/jcs.223776.supplemental

#### References

- Arasada, R. and Pollard, T. D. (2011). Distinct roles for F-BAR proteins Cdc15p and Bzz1p in actin polymerization at sites of endocytosis in fission yeast. Curr. Biol. 21, 1450-1459.
- Arasada, R. and Pollard, T. D. (2014). Contractile ring stability in S. pombe depends on F-BAR protein Cdc15p and Bgs1p transport from the Golgi complex. *Cell Rep.* 8, 1533-1544.
- Arellano, M., Durán, A. and Pérez, P. (1996). Rho 1 GTPase activates the (1-3)beta-D-glucan synthase and is involved in Schizosaccharomyces pombe morphogenesis. *EMBO J.* 15, 4584-4591.
- Attanapola, S. L., Alexander, C. J. and Mulvihill, D. P. (2009). Ste20-kinase-dependent TEDS-site phosphorylation modulates the dynamic localisation and endocytic function of the fission yeast class I myosin, Myo1. J. Cell Sci. 122, 3856-3861.
- Balasubramanian, M. K., McCollum, D., Chang, L., Wong, K. C., Naqvi, N. I., He, X., Sazer, S. and Gould, K. L. (1998). Isolation and characterization of new fission yeast cytokinesis mutants. *Genetics* 149, 1265-1275.
- Berro, J. and Lacy, M. M. (2018). Quantitative biology of endocytosis. *Colloquium Ser. Quant. Cell Biol.* **4**, 74.
- Bezanilla, M., Wilson, J. M. and Pollard, T. D. (2000). Fission yeast myosin-II isoforms assemble into contractile rings at distinct times during mitosis. *Curr. Biol.* 10, 397-400.
- Carnahan, R. H. and Gould, K. L. (2003). The PCH family protein, Cdc15p, recruits two F-actin nucleation pathways to coordinate cytokinetic actin ring formation in Schizosaccharomyces pombe. *J. Cell Biol.* **162**, 851-862.
- Chang, E. C., Barr, M., Wang, Y., Jung, V., Xu, H. P. and Wigler, M. H. (1994).
  Cooperative interaction of S. pombe proteins required for mating and morphogenesis. Cell 79, 131-141.
- Chang, F., Woollard, A. and Nurse, P. (1996). Isolation and characterization of fission yeast mutants defective in the assembly and placement of the contractile actin ring. *J. Cell Sci.* **109**, 131-142.
- Coffman, V. C., Sees, J. A., Kovar, D. R. and Wu, J.-Q. (2013). The formins Cdc12 and For3 cooperate during contractile ring assembly in cytokinesis. *J. Cell Biol.* 203, 101-114.
- Coll, P. M., Trillo, Y., Ametzazurra, A. and Perez, P. (2003). Gef1p, a new guanine nucleotide exchange factor for Cdc42p, regulates polarity in Schizosaccharomyces pombe. Mol. Biol. Cell 14, 313-323.
- Cortés, J. C. G., Ishiguro, J., Duran, A. and Ribas, J. C. (2002). Localization of the (1,3)beta-D-glucan synthase catalytic subunit homologue Bgs1p/Cps1p from fission yeast suggests that it is involved in septation, polarized growth, mating, spore wall formation and spore germination. *J. Cell Sci.* 115, 4081-4096.
- Cortés, J. C. G., Konomi, M., Martins, I. M., Muñoz, J., Moreno, M. B., Osumi, M., Durán, A. and Ribas, J. C. (2007). The (1,3)beta-D-glucan synthase subunit

- Bgs1p is responsible for the fission yeast primary septum formation. *Mol. Microbiol.* **65** 201-217
- Cortés, J. C. G., Pujol, N., Sato, M., Pinar, M., Ramos, M., Moreno, B., Osumi, M., Ribas, J. C. and Pérez, P. (2015). Cooperation between Paxillin-like protein Pxl1 and Glucan synthase Bgs1 is essential for actomyosin ring stability and septum formation in fission yeast. *PLoS Genet.* 11, e1005358.
- Das, M., Wiley, D. J., Chen, X., Shah, K. and Verde, F. (2009). The conserved NDR kinase Orb6 controls polarized cell growth by spatial regulation of the small GTPase Cdc42. Curr. Biol. 19, 1314-1319.
- Dorn, J. F., Zhang, L., Phi, T.-T., Lacroix, B., Maddox, P. S., Liu, J. and Maddox, A. S. (2016). A theoretical model of cytokinesis implicates feedback between membrane curvature and cytoskeletal organization in asymmetric cytokinetic furrowing. *Mol. Biol. Cell* 27, 1286-1299.
- Fankhauser, C., Reymond, A., Cerutti, L., Utzig, S., Hofmann, K. and Simanis, V. (1995). The S. pombe cdc15 gene is a key element in the reorganization of F-actin at mitosis. *Cell* 82, 435-444.
- Gachet, Y. and Hyams, J. S. (2005). Endocytosis in fission yeast is spatially associated with the actin cytoskeleton during polarised cell growth and cytokinesis. J. Cell Sci. 118, 4231-4242.
- Gao, L. and Bretscher, A. (2008). Analysis of unregulated formin activity reveals how yeast can balance F-actin assembly between different microfilament-based organizations. *Mol. Biol. Cell* 19, 1474-1484.
- Hachet, O. and Simanis, V. (2008). Mid1p/anillin and the septation initiation network orchestrate contractile ring assembly for cytokinesis. *Genes Dev.* 22, 3205-3216.
- Hirota, K., Tanaka, K., Ohta, K. and Yamamoto, M. (2003). Gef1p and Scd1p, the Two GDP-GTP exchange factors for Cdc42p, form a ring structure that shrinks during cytokinesis in Schizosaccharomyces pombe. *Mol. Biol. Cell* 14, 3617-3627.
- Huang, J., Huang, Y., Yu, H., Subramanian, D., Padmanabhan, A., Thadani, R., Tao, Y., Tang, X., Wedlich-Soldner, R. and Balasubramanian, M. K. (2012).
  Nonmedially assembled F-actin cables incorporate into the actomyosin ring in fission yeast. *J. Cell Biol.* 199, 831-847.
- Johnson, A. E., McCollum, D. and Gould, K. L. (2012). Polar opposites: fine-tuning cytokinesis through SIN asymmetry. Cytoskeleton 69, 686-699.
- Kamasaki, T., Osumi, M. and Mabuchi, I. (2007). Three-dimensional arrangement of F-actin in the contractile ring of fission yeast. *J. Cell Biol.* **178**, 765-771.
- Kitayama, C., Sugimoto, A. and Yamamoto, M. (1997). Type II myosin heavy chain encoded by the myo2 gene composes the contractile ring during cytokinesis in Schizosaccharomyces pombe. J. Cell Biol. 137, 1309-1319.
- Laplante, C., Berro, J., Karatekin, E., Hernandez-Leyva, A., Lee, R. and Pollard, T. D. (2015). Three myosins contribute uniquely to the assembly and constriction of the fission yeast cytokinetic contractile ring. *Curr. Biol.* 25, 1955-1965.
- Laporte, D., Zhao, R. and Wu, J.-Q. (2010). Mechanisms of contractile-ring assembly in fission yeast and beyond. Semin. Cell Dev. Biol. 21, 892-898.
- Laporte, D., Coffman, V. C., Lee, I.-J. and Wu, J.-Q. (2011). Assembly and architecture of precursor nodes during fission yeast cytokinesis. J. Cell Biol. 192, 1005-1021.
- Le Goff, X., Woollard, A. and Simanis, V. (1999). Analysis of the cps1 gene provides evidence for a septation checkpoint in Schizosaccharomyces pombe. Mol. Gen. Genet. 262, 163-172.
- Lee, I.-J., Coffman, V. C. and Wu, J.-Q. (2012). Contractile-ring assembly in fission yeast cytokinesis: recent advances and new perspectives. *Cytoskeleton* (Hoboken) **69**, 751-763.
- Liu, J., Wang, H., McCollum, D. and Balasubramanian, M. K. (1999). Drc1p/ Cps1p, a 1,3-beta-glucan synthase subunit, is essential for division septum assembly in Schizosaccharomyces pombe. *Genetics* 153, 1193-1203.
- Maddox, A. S., Lewellyn, L., Desai, A. and Oegema, K. (2007). Anillin and the septins promote asymmetric ingression of the cytokinetic furrow. Dev. Cell 12, 827-835
- Marcus, S., Polverino, A., Chang, E., Robbins, D., Cobb, M. H. and Wigler, M. H. (1995). Shk1, a homolog of the Saccharomyces cerevisiae Ste20 and mammalian p65PAK protein kinases, is a component of a Ras/Cdc42 signaling module in the fission yeast Schizosaccharomyces pombe. *Proc. Natl. Acad. Sci. USA* 92, 6180-6184.
- Marks, J., Fankhauser, C. and Simanis, V. (1992). Genetic interactions in the control of septation in Schizosaccharomyces pombe. J. Cell Sci. 101, 801-808.
- Martin-Garcia, R., Coll, P. M. and Perez, P. (2014). F-BAR domain protein Rga7 collaborates with Cdc15 and Imp2 to ensure proper cytokinesis in fission yeast. J. Cell Sci. 127, 4146-4158.
- McCollum, D., Feoktistova, A., Morphew, M., Balasubramanian, M. and Gould, K. L. (1996). The Schizosaccharomyces pombe actin-related protein, Arp3, is a component of the cortical actin cytoskeleton and interacts with profilin. *EMBO J.* 15, 6438-6446.
- McDonald, N. A., Vander Kooi, C. W., Ohi, M. D. and Gould, K. L. (2015). Oligomerization but not membrane bending underlies the function of certain F-BAR proteins in cell motility and cytokinesis. *Dev. Cell* **35**, 725-736.
- McDonald, N. A., Lind, A. L., Smith, S. E., Li, R. and Gould, K. L. (2017).
  Nanoscale architecture of the Schizosaccharomyces pombe contractile ring. eLife
  6, e28865.

- Moreno, S., Klar, A. and Nurse, P. (1991). Molecular genetic analysis of fission yeast Schizosaccharomyces pombe. *Methods Enzymol.* 194, 795-823.
- Morrell-Falvey, J. L., Ren, L., Feoktistova, A., Haese, G. D. and Gould, K. L. (2005). Cell wall remodeling at the fission yeast cell division site requires the Rho-GEF Rgf3p. J. Cell Sci. 118, 5563-5573.
- Mullins, R. D., Stafford, W. F. and Pollard, T. D. (1997). Structure, subunit topology, and actin-binding activity of the Arp2/3 complex from Acanthamoeba. J. Cell Biol. 136, 331-343.
- Mullins, R. D., Heuser, J. A. and Pollard, T. D. (1998). The interaction of Arp2/3 complex with actin: nucleation, high affinity pointed end capping, and formation of branching networks of filaments. *Proc. Natl. Acad. Sci. USA* 95, 6181-6186.
- Mulvihill, D. P. and Hyams, J. S. (2003). Role of the two type II myosins, Myo2 and Myp2, in cytokinetic actomyosin ring formation and function in fission yeast. *Cell Motil. Cytoskeleton* 54, 208-216.
- Muñoz, J., Cortés, J. C. G., Sipiczki, M., Ramos, M., Clemente-Ramos, J. A., Moreno, M. B., Martins, I. M., Pérez, P. and Ribas, J. C. (2013). Extracellular cell wall beta (1,3) glucan is required to couple septation to actomyosin ring contraction. J. Cell Biol. 203, 265-282.
- Mutoh, T., Nakano, K. and Mabuchi, I. (2005). Rho1-GEFs Rgf1 and Rgf2 are involved in formation of cell wall and septum, while Rgf3 is involved in cytokinesis in fission yeast. *Genes Cells* **10**, 1189-1202.
- Parrini, M. C., Lei, M., Harrison, S. C. and Mayer, B. J. (2002). Pak1 kinase homodimers are autoinhibited in trans and dissociated upon activation by Cdc42 and Rac1. Mol. Cell 9, 73-83.
- Pelham, R. J. and Chang, F. (2002). Actin dynamics in the contractile ring during cytokinesis in fission yeast. *Nature* 419, 82-86.
- Pollard, T. D. (2010). Mechanics of cytokinesis in eukaryotes. Curr. Opin. Cell Biol. 22, 50-56.
- **Pollard, T. D.** (2014). The value of mechanistic biophysical information for systems-level understanding of complex biological processes such as cytokinesis. *Biophys. J.* **107**, 2499-2507.
- Pollard, T. D. and Wu, J.-Q. (2010). Understanding cytokinesis: lessons from fission yeast. *Nat. Rev. Mol. Cell Biol.* 11, 149-155.
- Prekeris, R. and Gould, G. W. (2008). Breaking up is hard to do membrane traffic in cytokinesis. *J. Cell Sci.* **121**, 1569-1576.
- Proctor, S. A., Minc, N., Boudaoud, A. and Chang, F. (2012). Contributions of turgor pressure, the contractile ring, and septum assembly to forces in cytokinesis in fission yeast. *Curr. Biol.* 22, 1601-1608.
- Ren, L., Willet, A. H., Roberts-Galbraith, R. H., McDonald, N. A., Feoktistova, A., Chen, J.-S., Huang, H., Guillen, R., Boone, C., Sidhu, S. S. et al. (2015). The Cdc15 and Imp2 SH3 domains cooperatively scaffold a network of proteins that redundantly ensure efficient cell division in fission yeast. *Mol. Biol. Cell* 26, 256
- Roberts-Galbraith, R. H., Chen, J.-S., Wang, J. and Gould, K. L. (2009). The SH3 domains of two PCH family members cooperate in assembly of the Schizosaccharomyces pombe contractile ring. *J. Cell Biol.* **184**, 113-127.
- Roberts-Galbraith, R. H., Ohi, M. D., Ballif, B. A., Chen, J.-S., McLeod, I., McDonald, W. H., Gygi, S. P., Yates, J. R., Ill and Gould, K. L. (2010). Dephosphorylation of F-BAR protein Cdc15 modulates its conformation and stimulates its scaffolding activity at the cell division site. *Mol. Cell* 39, 86-99.
- Sladewski, T. E., Previs, M. J. and Lord, M. (2009). Regulation of fission yeast myosin-II function and contractile ring dynamics by regulatory light-chain and heavy-chain phosphorylation. *Mol. Biol. Cell* 20, 3941-3952.
- Stachowiak, M. R., Laplante, C., Chin, H. F., Guirao, B., Karatekin, E., Pollard, T. D. and O'Shaughnessy, B. (2014). Mechanism of cytokinetic contractile ring constriction in fission yeast. *Dev. Cell* 29, 547-561.

- Suarez, C., Carroll, R. T., Burke, T. A., Christensen, J. R., Bestul, A. J., Sees, J. A., James, M. L., Sirotkin, V. and Kovar, D. R. (2015). Profilin regulates F-actin network homeostasis by favoring formin over Arp2/3 complex. *Dev. Cell* 32, 43-53.
- Thiyagarajan, S., Munteanu, E. L., Arasada, R., Pollard, T. D. and O'Shaughnessy, B. (2015). The fission yeast cytokinetic contractile ring regulates septum shape and closure. J. Cell Sci. 128, 3672-3681.
- Tu, H. and Wigler, M. (1999). Genetic evidence for Pak1 autoinhibition and its release by Cdc42. *Mol. Cell. Biol.* 19, 602-611.
- Vjestica, A., Tang, X.-Z. and Oliferenko, S. (2008). The actomyosin ring recruits early secretory compartments to the division site in fission yeast. *Mol. Biol. Cell* 19, 1125-1138.
- Wachtler, V., Huang, Y., Karagiannis, J. and Balasubramanian, M. K. (2006).
  Cell cycle-dependent roles for the FCH-domain protein Cdc15p in formation of the actomyosin ring in Schizosaccharomyces pombe. *Mol. Biol. Cell* 17, 3254-3266.
- Wang, N., Lee, I.-J., Rask, G. and Wu, J.-Q. (2016). Roles of the TRAPP-II complex and the exocyst in membrane deposition during fission yeast cytokinesis. *PLoS Biol.* 14, e1002437.
- Wei, B., Hercyk, B. S., Mattson, N., Mohammadi, A., Rich, J., DeBruyne, E., Clark, M. M. and Das, M. (2016). Unique spatiotemporal activation pattern of Cdc42 by Gef1 and Scd1 promotes different events during cytokinesis. *Mol. Biol. Cell* 27, 1181-1407.
- Wei, B., Hercyk, B. S., Habiyaremye, J. and Das, M. (2017). Spatiotemporal analysis of cytokinetic events in fission yeast. *J. Vis. Exp.* **120**, e55109.
- Welch, M. D., Iwamatsu, A. and Mitchison, T. J. (1997). Actin polymerization is induced by Arp2/3 protein complex at the surface of Listeria monocytogenes. *Nature* 385, 265-269.
- Willet, A. H., McDonald, N. A., Bohnert, K. A., Baird, M. A., Allen, J. R., Davidson, M. W. and Gould, K. L. (2015). The F-BAR Cdc15 promotes contractile ring formation through the direct recruitment of the formin Cdc12. *J. Cell Biol.* 208, 391-399.
- Win, T. Z., Gachet, Y., Mulvihill, D. P., May, K. M. and Hyams, J. S. (2001). Two type V myosins with non-overlapping functions in the fission yeast Schizosaccharomyces pombe: Myo52 is concerned with growth polarity and cytokinesis, Myo51 is a component of the cytokinetic actin ring. *J. Cell Sci.* 114, 69-79.
- Winter, D., Podtelejnikov, A. V., Mann, M. and Li, R. (1997). The complex containing actin-related proteins Arp2 and Arp3 is required for the motility and integrity of yeast actin patches. Curr. Biol. 7, 519-529.
- Wu, J.-Q. and Pollard, T. D. (2005). Counting cytokinesis proteins globally and locally in fission yeast. Science 310, 310-314.
- Wu, J.-Q., Bähler, J. and Pringle, J. R. (2001). Roles of a fimbrin and an alphaactinin-like protein in fission yeast cell polarization and cytokinesis. *Mol. Biol. Cell* 12, 1061-1077.
- Wu, J.-Q., Kuhn, J. R., Kovar, D. R. and Pollard, T. D. (2003). Spatial and temporal pathway for assembly and constriction of the contractile ring in fission yeast cytokinesis. *Dev. Cell* 5, 723-734.
- Wu, J.-Q., Sirotkin, V., Kovar, D. R., Lord, M., Beltzner, C. C., Kuhn, J. R. and Pollard, T. D. (2006). Assembly of the cytokinetic contractile ring from a broad band of nodes in fission yeast. J. Cell Biol. 174, 391-402.
- Zhou, Z., Munteanu, E. L., He, J., Ursell, T., Bathe, M., Huang, K. C. and Chang, F. (2015). The contractile ring coordinates curvature-dependent septum assembly during fission yeast cytokinesis. *Mol. Biol. Cell* 26, 78-90.

**Table S1. Strains list** 

| Strain   | Genotype  | Origin                           |
|----------|---|----------------------------------|
| PN975    | h+ ura4-D18 leu1-32 ade6-704  | P. Nurse                         |
| MBY6843  | h+ lifeact-mCherry: leu+ ade6-M216 leu1-32 ura4-D18   | (Huang et al.,<br>2012)          |
| YMD17    | h- Δgef1::ura4+ lifeact-mCherry: leu+ ade6-M216 leu1-<br>32 ura4-D18  | This study                       |
| YMD449   | Δgef1::ura4+ lifeact-mCherry: leu+ ura4+ -Pcdc12-∆503-cdc12 ade6-M21* leu1-32 ura4-D18 ura4-D18                                     | This study                       |
| YMD453   | h+ lifeact-mCherry: leu+ ade6-M21* leu1-32 ura4-D18 ura4⁺-Pcdc12-∆503-cdc12   | This study                       |
| KGY3019  | cdc15-GFP: kanMX6 ade6-M210 leu1-32 ura4-D18  | (Carnahan and<br>Gould, 2003)    |
| JW1711   | h- ura4 <sup>+</sup> -Pcdc12-∆503-cdc12 ade6-M210 leu1-32 ura4-<br>D18  | (Coffman et al., 2013)           |
| YMD387   | ura4⁺-Pcdc12-∆503-cdc12 cdc15-GFP: kanMX6 ade6-<br>M210 leu1-32 ura4-D18  | This study                       |
| YMD131   | Δgef1::ura4+cdc15-GFP: kanMX6 sad1-mCherry:kanMX ade6-M21X leu1-32 ura4-D18   | This study                       |
| YMD134   | h+ cdc15-GFP: kanMX6 sad1-mCherry: kanMX ade6-<br>M21X leu1-32 ura4-D18   | This study                       |
| YMD394   | Δgef1::ura4 <sup>+</sup> ura4 <sup>+</sup> -Pcdc12-∆503-cdc12 cdc15-GFP:<br>kanMX6 ura4 <sup>-</sup> D18 leu1-32 ade6-M210          | This study                       |
| YMD473   | Δgef1::ura4+ pjk148-nmt41x-leu1+ cdc15-GFP: kanMX6 sad1-mCherry:KanMX6 ade6 leu1-32 ura4-D18  | This study                       |
| YMD474   | Δgef1::ura4 <sup>+</sup> pjk148-nmt41x-cdc42G12V-leu <sup>+</sup> cdc15-<br>GFP: kanMX6 sad1-mCherry:KanMX ade6 leu1-32<br>ura4-D18 | This study                       |
| YMD498   | cdc15-GFP:kanMX6 sad1-mCherry:kanMX ade6-M21X leu1-32 ura4-D18 pjk148-nmt41x-leu1*  | This study                       |
| PPG3750  | h- Δbgs1::ura4 Pbgs1::GFP-bgs1:leu1* leu1-32 ura4-<br>D18 his3-D1   | (Cortes et al.,<br>2007)         |
| YMD546   | Δbgs1::ura4 <sup>+</sup> Pbgs1::GFP-bgs1:leu1 <sup>+</sup> rlc1-tdTomato-<br>NAT <sup>r</sup> sad1-mCherry:kanMX leu1-32 ura4-D18   | This study                       |
| KGY6899  | h- cdc15::cdc15∆SH3-GFP:kanR ade6-M210 ura4-D18 leu1-32   | (Roberts-Galbraith et al., 2009) |
| YMD917   | h+ cdc15::cdc15∆SH3-GFP:kanR sad1-mCherry:kanMX ade6-M210 ura4-D18 leu1-32  | This study                       |
| YMD891   | Δgef1::ura4 <sup>+</sup> cdc15::cdc15∆SH3-GFP:kanR sad1-<br>mCherry:kanMX ade6-M210 ura4-D18 leu1-32                                | This study                       |
| YMD527   | rlc1-tdTomato-NAT <sup>r</sup> sad1-mCherry: kanMx ade6-M21X<br>leu1-32 his7+ ura4-D18  | This study                       |
| KGY13149 | h- cdc12-P31A:kanR ade6-M210 leu1-32 ura4-D18   | (Willet et al.,<br>2015)         |
| YMD192   | cdc15-tomato-NAT <sup>r</sup> ade6-M216 leu1-32 ura4-D18 his7   | This study                       |
| YMD591   | Δgef1::ura4 <sup>+</sup> cdc15-tomato-NAT <sup>r</sup> ade6-M216 leu1-32<br>ura4-D18 his7   | This study                       |
| YMD656   | cdc12-P31A:kanR ade6-M210 leu1-32 ura4-D18  | This study                       |

| YMD657  | Δgef1::ura4 <sup>+</sup> cdc12-P31A:kanR ade6-M210 leu1-32<br>ura4-D18       | This study              |
|---------|--|-------------------------|
| FV1     | h+ orb2-34 ade6 M216 leu1-32   | (Verde et al.,<br>1995) |
| YMD767  | orb2-34 cdc15-GFP: kanMX6 ade6-M216 leu1-32                                  | This study              |
| YMD736  | orb2-34 ura4⁺-Pcdc12-∆503-cdc12 cdc15-GFP: kanMX6 ade6-M21* leu1-32 ura4-D18 | This study              |
| KGY680  | h+ arp3-C1 leul-32 ura4-D18 his3-237   | Mccollum et al.,1996),  |
| YMD1148 | arp3-C1 cdc15-GFP:kanMX6 sad1-mCherry:kanMX ade6-M21X leu1-32 ura4-D18 his?  | This study              |

### Table S2. Number of Cdc15 proteins at the ring during maturation

|                               | gef1+cdc12+ | gef1∆ | cdc12∆503 | gef1Δ<br>cdc12Δ503 |
|-------------------------------|-------------|-------|-----------|--------------------|
| Total protein at t=20 minutes | 2500        | 2500  | 1760      | 1820               |

#### **REFERENCES**

- Carnahan, R.H., and K.L. Gould. 2003. The PCH family protein, Cdc15p, recruits two F-actin nucleation pathways to coordinate cytokinetic actin ring formation in Schizosaccharomyces pombe. *J Cell Biol*. 162:851-862.
- Coffman, V.C., J.A. Sees, D.R. Kovar, and J.Q. Wu. 2013. The formins Cdc12 and For3 cooperate during contractile ring assembly in cytokinesis. *J Cell Biol*. 203:101-114.
- Cortes, J.C., M. Konomi, I.M. Martins, J. Munoz, M.B. Moreno, M. Osumi, A. Duran, and J.C. Ribas. 2007. The (1,3)beta-D-glucan synthase subunit Bgs1p is responsible for the fission yeast primary septum formation. *Mol Microbiol*. 65:201-217.
- Huang, J., Y. Huang, H. Yu, D. Subramanian, A. Padmanabhan, R. Thadani, Y. Tao, X. Tang, R. Wedlich-Soldner, and M.K. Balasubramanian. 2012. Nonmedially assembled F-actin cables incorporate into the actomyosin ring in fission yeast. *J Cell Biol*. 199:831-847.
- Roberts-Galbraith, R.H., J.S. Chen, J. Wang, and K.L. Gould. 2009. The SH3 domains of two PCH family members cooperate in assembly of the Schizosaccharomyces pombe contractile ring. *J Cell Biol.* 184:113-127.
- Verde, F., J. Mata, and P. Nurse. 1995. Fission yeast cell morphogenesis: identification of new genes and analysis of their role during the cell cycle. *The Journal of cell biology*. 131:1529-1538.
- Willet, A.H., N.A. McDonald, K.A. Bohnert, M.A. Baird, J.R. Allen, M.W. Davidson, and K.L. Gould. 2015. The F-BAR Cdc15 promotes contractile ring formation through the direct recruitment of the formin Cdc12. *J Cell Biol.* 208:391-399.

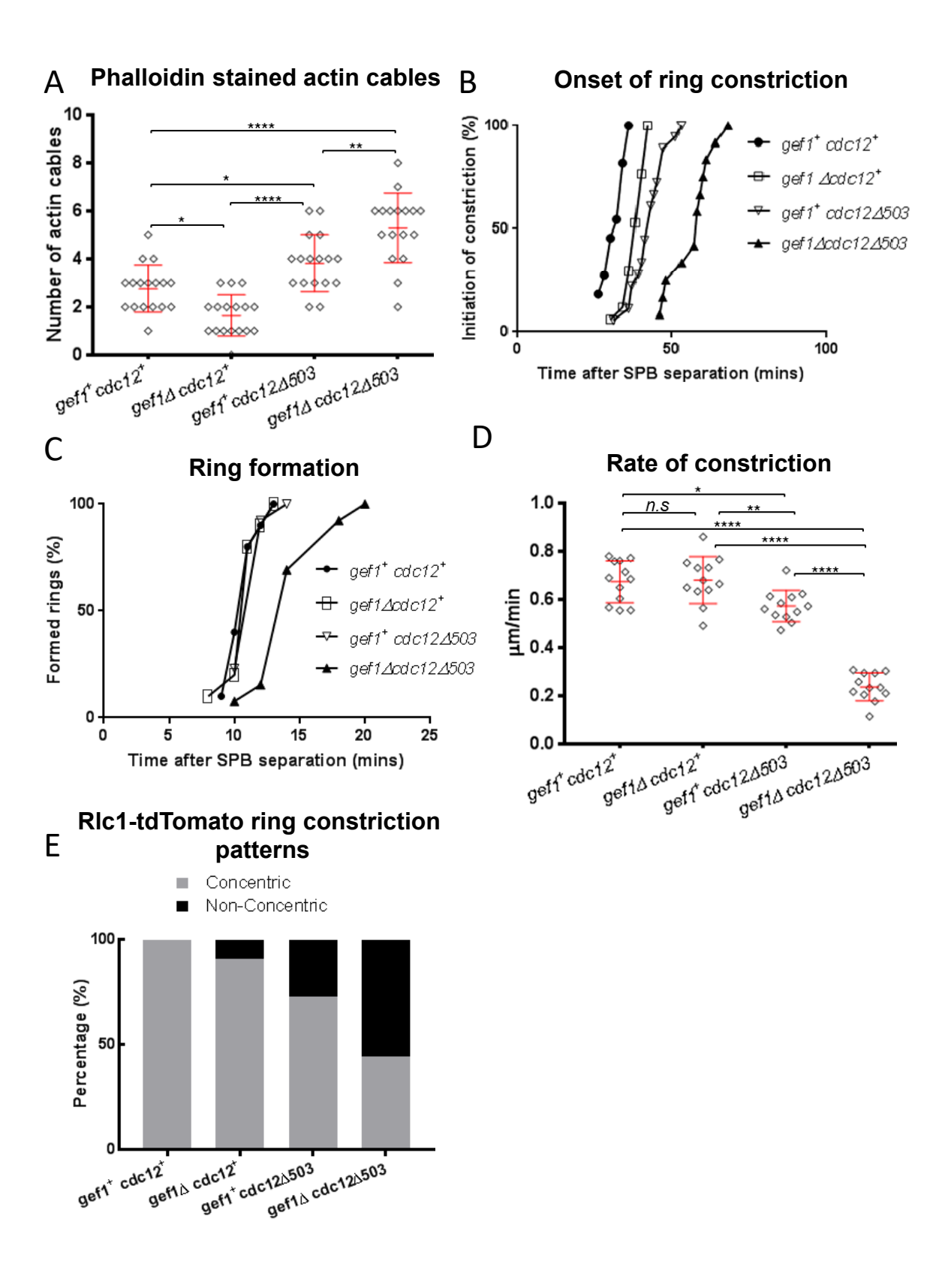


## Figure S1. Actomyosin ring constriction defects are more severe in $gef1\Delta$ mutants expressing an activated formin allele $cdc12\Delta503$ .

**(A).**Quantification of phalloidin stained non-medial actin cables in strains as indicated,  $[n \ge 17 \text{ cells}]$ ; one-way ANOVA, (F(3, 64) = 31.67 p < 0.0001), with Tukey's multiple comparisons post hoc test, n.s-not significant,  $p \le 0.05$ ,  $p \le 0.001$ . **(B).** Outcome plot showing percentage of cells with Cdc15-GFP labelled rings initiating constriction in the indicated strains  $[n \ge 11 \text{ cells}]$ . **(C).** Outcome plot with the percentage of Cdc15-GFP labelled actomyosin rings formed in the indicated strains. **(D).** Quantification of the rate of ring constriction in the indicated strains, [n = 12 cells]; one-way ANOVA, [n = 12 cells]; one-way ANOVA, [n = 12 cells], with Tukey's multiple comparisons post hoc test, [n = 12 cells], [n = 12 cells]. Quantification of the percentage of non-concentric furrow formation observed in Rlc1-tdTomato labelled rings in the indicated strains,  $[n \ge 9 \text{ cells}]$ .

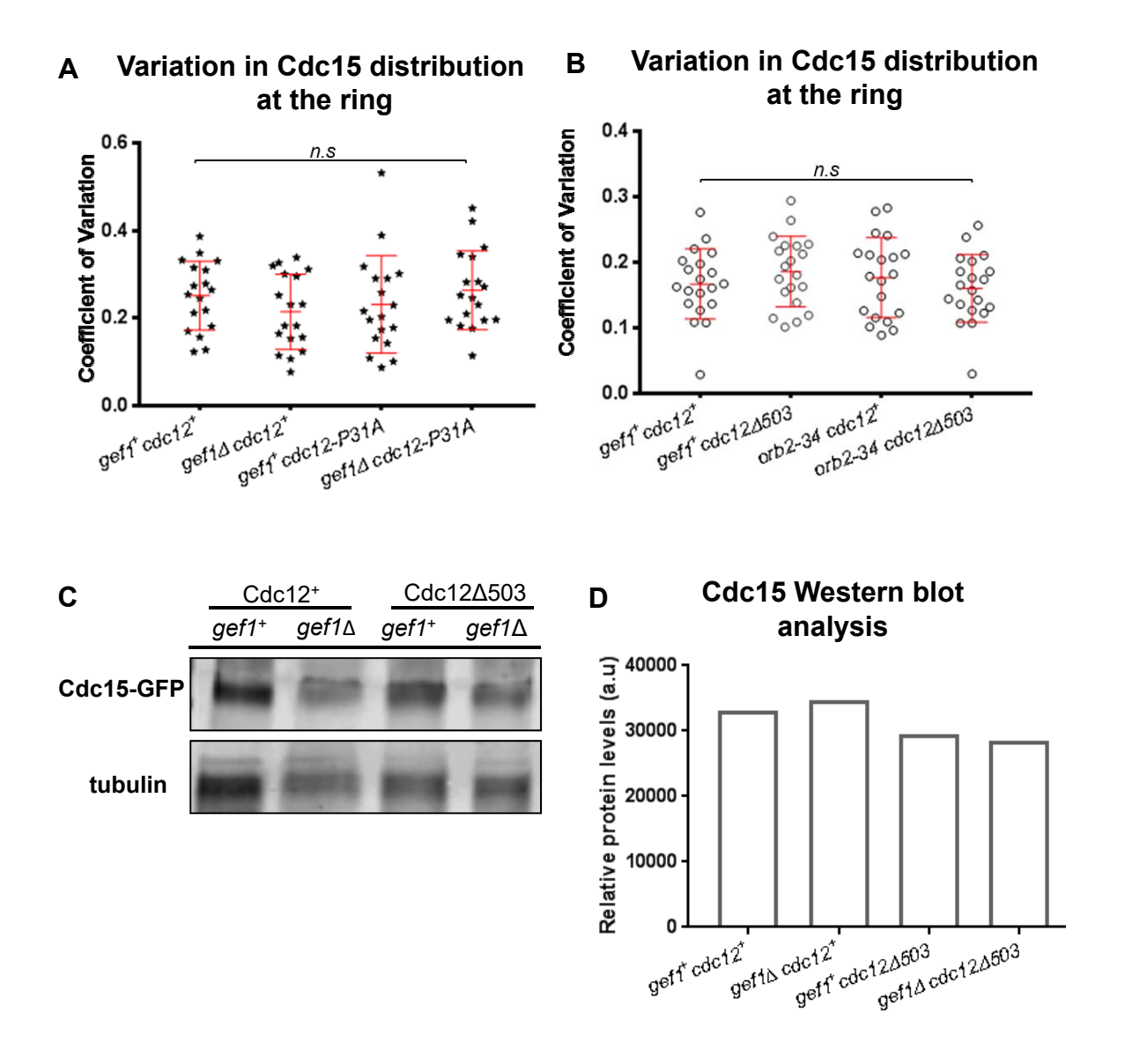


**Figure S2. (A).** Coefficient of Variation of Cdc15-GFP distribution along the ring in the indicated strains [n=18;one-way ANOVA (F (3, 68) = 0.9971 p=0.3996), with Tukey's multiple comparisons post hoc test, *n.s.-not significant*]. **(B).** Coefficient of Variation of Cdc15-GFP distribution along the ring in the indicated strains, [n=20;one-way ANOVA (F (3, 76) = 0.8313 p=0.4808), with Tukey's multiple comparisons post hoc test, *n.s.-not significant*]. **(C).** Western blot showing Cdc15-GFP and Tubulin (control). **(D).** Quantification of relative Cdc15 levels from Western blot. Error bars represent standard deviation.

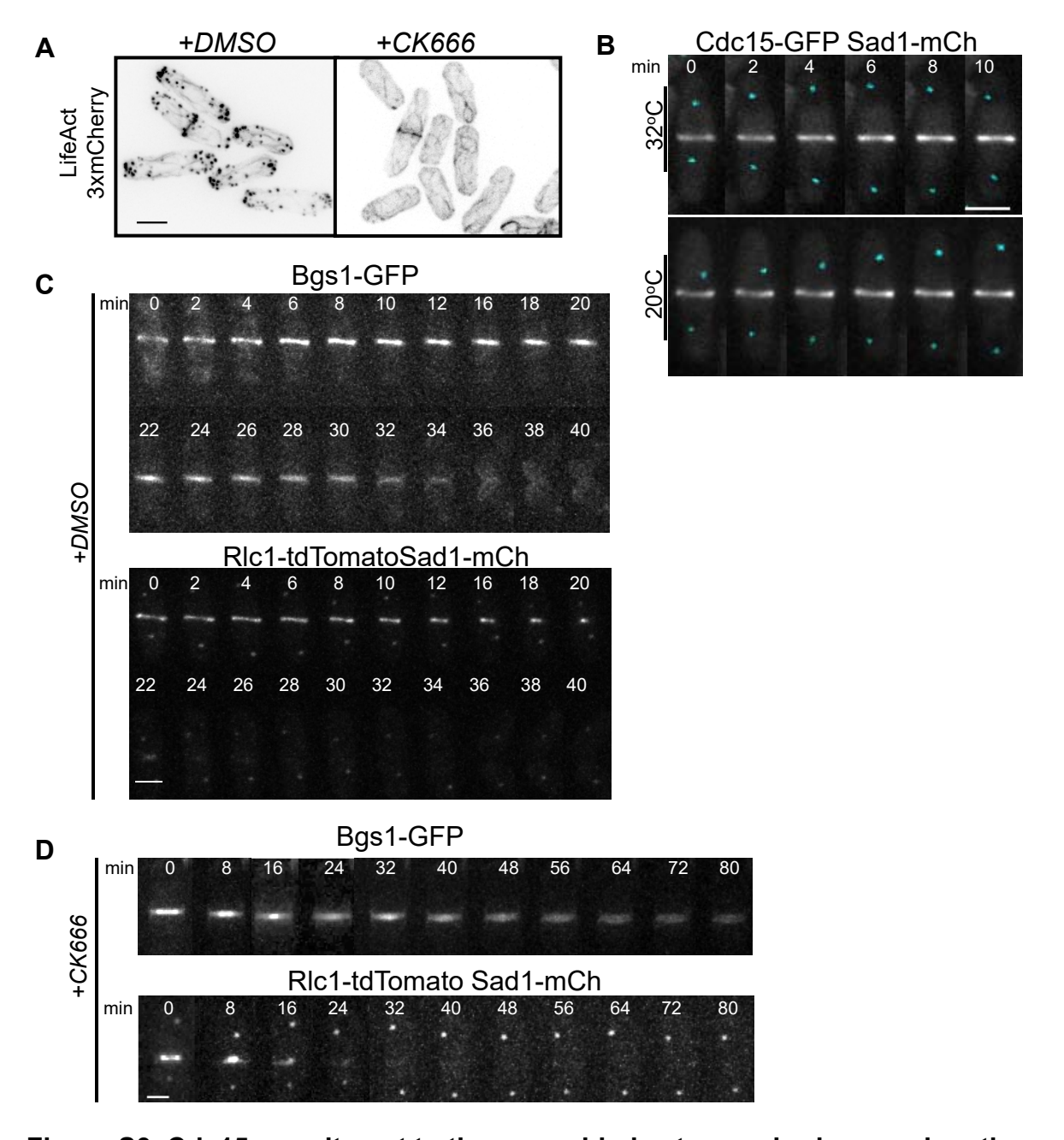
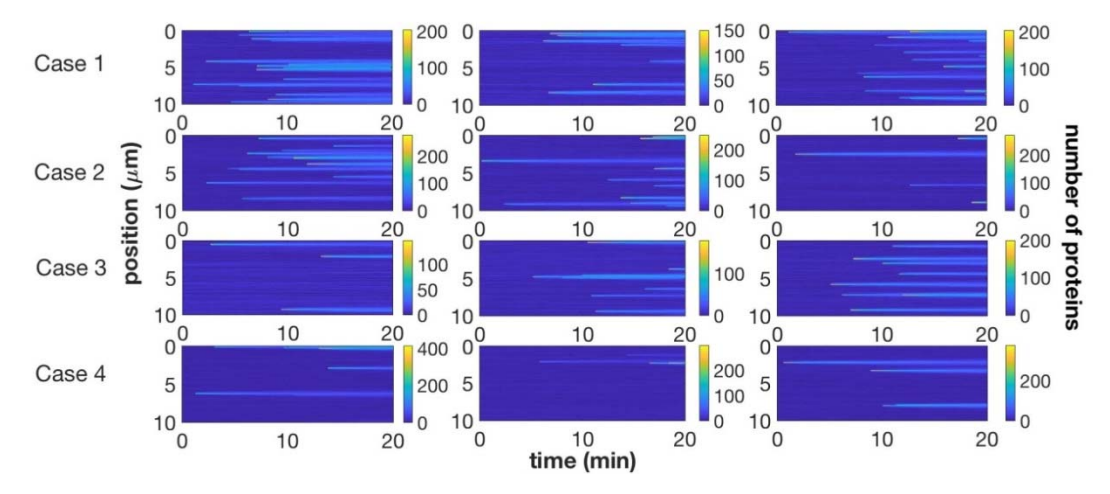


**Figure S3.** Cdc15 recruitment to the assembled actomyosin ring requires the Arp2/3 complex. (A). Cells expressing Life-Act-3xmCherry, treated with DMSO or 100uM of CK666. (B). Control experiment for fig. 5F showing time-lapse images of *arp3*+ cells expressing Cdc15-GFP at permissive and non-permissive temperatures. (C). Cell separation observed in DMSO treated cells expressing Bgs1-GFP, Rlc1-tdTomato and Sad1-mCherry. (D). CK666 treated cells expressing Bgs1-GFP, Rlc1-tdTomato and Sad1-mCherry fail to undergo cell separation; scale bars =5μm.





| Patch associ<br>mo | ation rate constant (k <sub>pa</sub><br>lecules associated with | <sub>tch</sub> ) and number of Cdc15<br>a patch (N <sub>patch</sub> ) |
|--------------------|---|---|
| Case #             | k <sub>patch</sub> (min <sup>-1</sup> )                         | N <sub>patch</sub>  |
| 1                  | 0.77  | 130 ± 43  |
| 2                  | 0.51  | 194 ± 69  |
| 3                  | 0.41  | 152 ± 46  |
| 4                  | 0.27  | 243 ± 98  |

**Figure S4. (A).** Kymographs over 20 minutes for 3 independent simulated rings for each of the 4 simulated cases; the vertical axis represents the position along the circumference of the ring and the color represents the number of Cdc15 proteins at that position and time. The spatial distribution of proteins for each of these simulated rings is shown in Figure 7B. **(B).** The  $k_{patch}$  values used are designed to produce a final Cdc15 population after 20 minutes that is similar to the population observed experimentally in a mature ring.